Loss of *Cntnap2* causes axonal excitability deficits, developmental delay in cortical myelination, and abnormal stereotyped motor behavior

Ricardo Scott[1,8], Alberto Sánchez-Aguilera[2,3,8], Kim van Elst[4,8], Lynette Lim[2,3], Nathalie Dehorter[2], Sung Eun Bae[2,3], Giorgia Bartolini[1,2], Elior Peles[5], Martien J. H. Kas[4,6], Hilgo Bruining[7] and Oscar Marín[1,2,3]

[1]Instituto de Neurociencias, Consejo Superior de Investigaciones Científicas & Universidad Miguel Hernández, Sant Joan d'Alacant 03550, Spain
[2]Centre for Developmental Neurobiology, Institute of Psychiatry, Psychology and Neuroscience, King's College London, London SE1 1UL, United Kingdom
[3]MRC Centre for Neurodevelopmental Disorders, King's College London, London SE1 1UL, United Kingdom
[4]Department of Translational Neuroscience, Brain Center Rudolf Magnus, University Medical Center Utrecht, Utrecht University, the Netherlands
[5]Department of Molecular Cell Biology, Weizmann Institute of Science, Rehovot 7610001, Israel
[6]Groningen Institute for Evolutionary Life Sciences, University of Groningen, the Netherlands
[7]Department of Psychiatry, Brain Center Rudolf Magnus, University Medical Center Utrecht, the Netherlands
[8]These authors contribute equally to this work

Address correspondence to O. Marín. Email: oscar.marin@kcl.ac.uk
Running title: Abnormal axonal excitability in *Cntnap2* mouse mutants

Abstract

Contactin-associated protein-like 2 (Caspr2) is found at the nodes of Ranvier and has been associated with physiological properties of white matter conductivity. Genetic variation in *CNTNAP2*, the gene encoding Caspr2, has been linked to several neurodevelopmental conditions, yet pathophysiological effects of *CNTNAP2* mutations on axonal physiology and brain myelination are unknown. Here we have investigated mouse mutants for *Cntnap2* and found profound deficiencies in the clustering of Kv1-family potassium channels in the juxtaparanodes of brain myelinated axons. These deficits are associated with a change in the waveform of axonal action potentials and increases in postsynaptic excitatory responses. We also observed that the normal process of myelination is delayed in *Cntnap2* mutant mice. This later phenotype is a likely modulator of the developmental expressivity of the stereotyped motor behaviors that characterize *Cntnap2* mutant mice. Altogether, our results reveal a mechanism linked to white matter conductivity through which mutation of *CNTNAP2* may affect neurodevelopmental outcomes.

Keywords: Caspr2, axonal action potentials, myelin, Kv1-family potassium channels, GABAergic interneurons

Human genetic studies have revealed significant overlaps in genetic variation contributing to multiple neuropsychiatric disorders (Cross-Disorder Group of the Psychiatric Genomics et al. 2013; Guilmatre et al. 2014; McCarthy et al. 2014). One of such examples is variation in CNTNAP2, a member of the neurexin superfamily that has been linked to several neurodevelopmental disorders (Rodenas-Cuadrado et al. 2014; Poot 2015). In particular, genetic variation in the CNTNAP2 locus has been associated with childhood apraxia of speech and language impairments, intellectual disability, autism spectrum disorder (ASD), epilepsy and schizophrenia (Strauss et al. 2006; Friedman et al. 2008; Worthey et al. 2013; Centanni et al. 2015). Although it has been shown that different mutations in the same gene may cause functionally distinct phenotypes (Zhou et al. 2016), the association of a single gene to neurodevelopmental disorders may also be indicative of common pathophysiology (De Rubeis et al. 2014; Fromer et al. 2014). In the case of CNTNAP2, the biological mechanisms underlying the contribution of this gene to the developmental trajectory of neuropsychiatric disorders remain unclear (Scott-Van Zeeland et al. 2010; Dennis et al. 2011).

Animal model studies have so far mostly focused on analyzing the consequences of disrupting CNTNAP2 function on the balance between excitatory and inhibitory circuits. For example, it has been reported that deficits in the distribution of inhibitory GABAergic neurons may underlie the behavioral alterations found in both mouse and zebrafish Cntnap2 mutants (Peñagarikano et al. 2011; Hoffman et al. 2016). In mice, loss of cortical GABAergic interneurons has been associated with defects in neural synchronization (Peñagarikano et al. 2011), which reinforces the view that disruption of the excitatory/inhibitory balance might be at the core of the behavioral deficits observed in Cntnap2 mutants (Peñagarikano et al. 2011; Anderson et al. 2012; Gdalyahu et al. 2015;

Jurgensen and Castillo 2015; Varea et al. 2015). In addition, it has been suggested that CNTNAP2 may play a role in synapse development and function (Anderson et al. 2012; Gdalyahu et al. 2015; Varea et al. 2015).

Somehow surprisingly, the most established role for *CNTNAP2* has not yet been considered in the context of neurodevelopmental disorders. *CNTNAP2* encodes Contactin-associated protein-like 2 (Caspr2), a cell-cell adhesion molecule widely expressed throughout the brain (Gordon et al. 2016) that localizes to the juxtaparanodal region adjacent to the nodes of Ranvier in myelinated axons, where it mediates the interaction between myelinating glia and the axonal membrane (Poliak et al. 2001; Traka et al. 2003). Caspr2 is required for the clustering of Kv1-family potassium channels at this precise subcellular location (Poliak et al. 1999; Poliak et al. 2003; Traka et al. 2003), which are important to stabilize the conduction of axon potentials (Zhou et al. 1998; Vabnick et al. 1999). Caspr2 is also expressed in the axon initial segment (Inda et al. 2006) but, in contrast to the juxtaparanodes, its function seems dispensable for the clustering of potassium channels in this subcellular region (Ogawa et al. 2008). Based on these observations, it remains to be established whether *Cntnap2* disruption may cause neurodevelopmental deficits through disruption of axonal action potential dynamics or aberrant brain myelination. Their study is of importance to gain understanding of reduced white matter integrity and conductivity implicated in neurodevelopmental disorders (Vissers et al. 2012; Rane et al. 2015; Wolff et al. 2015; Fingher et al. 2017).

Here, we investigated axonal physiological properties and postnatal development of myelination in comparison to the emergence of neurophysiological, cognitive, neurological and behavioral deficits in *Cntnap2* mouse mutants. Our results suggest that defects in the propagation of action potentials along myelinated axons contribute to the functional

deficits observed in the absence of Caspr2. These results reveal a previously unanticipated role for myelination in this process and provide a plausible explanation for the developmental trajectory of the predominantly motor behavioral abnormalities observed in *Cntnap2* mutants. Our findings establish a pervasive mechanism through which CNTNAP2 mutations may predispose to a spectrum of neurodevelopmental conditions.

Materials and Methods

Animals

This study was performed in strict accordance with regulation in Spanish, British, Dutch and European Union regulations. Mice were weaned at postnatal (P) day 21, ear punched for genotyping and identification, and socially housed with littermates in groups of 2-5 mice per cage. Mice carrying loss of function *Cntnap2* alleles (Poliak et al. 2003) (hereafter called *Cntnap2* mutants) were maintained in a C57BL/6J background.

Histology

Postnatal mice were perfused transcardially with 4% PFA in PBS and the dissected brains were fixed for 2 h at 4°C in the same solution. Brains were sectioned at 60 μm on a vibratome or 40 μm on a freezing microtome and free-floating coronal sections were then subsequently processed for immunohistochemistry as previously described (Pla et al. 2006). The following primary antibodies were used: mouse anti-Ankyrin G (1:500, NeuroMab 75-146), rabbit anti-Calretinin (1:1000, Swant 7697), rabbit anti-Caspr (1:500), mouse anti-Caspr (1:300, NeuroMab 75-001); mouse anti-Caspr2 (1:400), rat anti-Ctip2 (1:500, Abcam ab18465), rabbit anti-Cux1 (1:100, Santa-Cruz CDP-M222), chicken anti-GFP (1:1000, Aves Labs GFP-1020), mouse anti-Kv1.2 potassium channel subunit (1:400, NeuroMab 73-008), mouse anti-Kv1.2 potassium channel subunit (a kind gift from M. N. Rasband), mouse anti-Myelin basic protein (1:500, Merck Millipore MAB384), rabbit anti-Parvalbumin (1:1000, Swant PV27), rabbit anti-Sodium channel (1:300, Sigma-Aldrich S6936), guinea pig anti-Sox10 (a kind gift from M. Wegner), and rat anti-Somatostatin (1:200, Millipore MAB354).

Electrophysiology

Juvenile (3-4 weeks), adolescent (6-9 weeks) and adult (10-12 weeks) mice were used to prepare acute brain slices. Juvenile animals were anesthetized with pentobarbital and transcardially perfused with cold 95% O_2 + 5% CO_2 sucrose artificial cerebrospinal fluid (aCSF). Coronal slices (350 μm) were cut using a Leica vibratome (Leica VT 1200S). Then, they were stored at room temperature for at least 1 hour in a submerged holding chamber with 95% O_2/5% CO_2 recording aCSF. For adult animals, we prepared slices (300 μm) as described before (Ting et al. 2014) with small modifications. Recordings were performed at 22-24°C.

For extracellular recordings, stimulation of the corpus callosum was performed with a bipolar stimulating electrode (tungsten wires, 75 μm tip separation, 2 MΩ, WPI), and voltage pulses of 20-30 μs were applied each 30 s by ISO STIM 01D (NPI Electronic). Antagonists were applied to the recording aCSF to block the synaptic transmission: NBQX (50 μM), picrotoxin (100 μM), AP5 (50 μM) and CGP52432 (5 μM). Somatic patch-clamp recordings in whole-cell configuration were made from cortical layer 2/3 pyramidal neurons under visual guidance with infrared-differential interference optics (Olympus U-TLUIR) through a 40x water-immersion objective. Excitatory currents were recorded at a holding potential of –70 mV (close to the chloride equilibrium potential) and inhibitory currents at +10 mV (reversal potential of glutamatergic events). For the recordings of miniature currents, tetrodotoxin (1 μM, Alomone Laboratories) was applied to the extracellular solution. For the intracellular recordings of evoked currents in layer 2/3 pyramidal neurons, stimulation of the corpus callosum was performed with a bipolar stimulating electrode (tungsten wires, 75 μm tip separation, 2 MΩ, WPI) positioned under visual control on the callosal tract as described earlier (Kumar and Huguenard 2001) while

the membrane potential was held at –70 mV. To exclusively study excitatory responses and to reduce polysynaptic signals, picrotoxin (100 μM) was included in the recording aCSF to block all $GABA_A$-receptor-mediated responses.

Image analysis and quantification

For the quantification of cell distributions, each animal is considered a biological replication (n). For each animal, about 10 to 12 sections or imaging field were imaged and treated as technical replicates within the somatosensory cortex and imaged with appropriate excitation and emission requirement based upon the staining used. All images were analyzed with customized software written in MATLAB (Mathworks). Layers were defined following nuclear staining.

Behavior

A suite of behavioral paradigms was used to test the developmental onset of abnormalities in male *Cntnap2* mutant mice (Supplementary Fig. 1). All mice were bred and housed under a 12h light-dark cycle (lights on from 19:00-07:00). Before each behavioral experiment, animals were transferred to the test-room and habituated for at least one hour prior to testing. The same sets of mice were tested longitudinally, from early adolescence until adulthood. Details of the behavioral paradigms can be found in the supplementary methods.

Statistical analyses

Statistical analysis was carried out with IBM SPSS Statistics. P values below 0.05 were considered statistically significant. Data are presented as mean and SEM throughout the manuscript (Supplementary Table 1*)*. Individual trial differences in behavior were determined using one-way ANOVA to test genotype effects. For repeated measurements, a

repeated measures ANOVA was performed with 'time' as within-subjects factor and 'genotype' as between-subjects factor. In case of a significant *p* value, post-hoc comparisons were performed using one-way ANOVA to determine individual time point effects. The involuntary movements and SHIRPA scores were not normally distributed and therefore compared using the general linear model. Normality and variance tests were first applied to all experimental data. When data followed a normal distribution, paired comparisons were analyzed with *t*-test, while multiple comparisons were analyzed using either ANOVA with post-hoc Bonferroni correction (equal variances) or the Welch test with *post-hoc* Games-Howell (different variances). A χ^2-test was applied to analyze the distribution of cells in layers.

Results

Disrupted clustering of potassium channels in the brain of *Cntnap2* mutant mice

Caspr2 has been previously shown to be required for the normal clustering of potassium channels in the juxtaparanodal region of the nodes of Ranvier in myelinated peripheral axons (Poliak et al. 2003). We wondered whether a similar defect was present in long-range cortical axons, which are also densely myelinated (Tomassy et al. 2014). In 8 weeks old mice, Caspr2 expression is abundant in the corpus callosum, which primarily comprise interhemispheric axons from pyramidal cells located in superficial layers of the cortex (Fig. 1A, B). At the subcellular level, Caspr2 is found in the juxtaparanodal region of the nodes of Ranvier (Fig. 1C, D, E), immediately flanking the paranodal junction. As reported earlier in peripheral nervous system axons (Poliak et al. 2003), we observed that Caspr and sodium channels are properly located at the paranodal junction and the nodes, respectively, in *Cntnap2* mutants (Fig. 1C, D–G). In contrast, clustering of Kv1.2 channels is severely disrupted in cortical myelinated axons in the corpus callosum of *Cntnap2* mutant mice compared to controls (Fig. 1H–K). We observed a prominent reduction in the number of nodes containing symmetric Kv1.2 clusters and a parallel increase in the frequency of nodes with asymmetric clusters or with complete absence of Kv1.2 clusters (Fig. 1L). Similar defects were observed in other regions of the telencephalon, including the internal capsule traversing the striatum and the external capsule (data not shown). Altogether, these results revealed that the organization of potassium channels in brain myelinated axons is severely disrupted in *Cntnap2* mutant mice.

Abnormal axonal action potential waveform in *Cntnap2* mutant mice

The functional consequences of the abnormal clustering of potassium channels in the juxtaparanodal region of the nodes of Ranvier are poorly understood. Previous studies in both optic and sciatic nerves of adult *Cntnap2* mutant mice revealed no apparent changes in nerve conduction (Poliak et al. 2003). However, the absence of clustered potassium channels at the nodes of Ranvier is expected to have an impact in action potential waveform and axonal excitability (Vabnick et al. 1999; Vivekananda et al. 2017). To test this hypothesis, we investigated global axonal electrical activity in acute cortical slices from 8 weeks old mice. To this end, we first stimulated the corpus callosum in one hemisphere and recorded the fiber volleys (FV) evoked from the contralateral hemisphere (Fig. 2A). We observed that FV amplitudes are significantly reduced in *Cntnap2* mutant mice compared to controls (Fig. 2B, C), indicative of changes in axonal action potential waveform, fiber recruitment or axonal density. Analysis of the distribution of pyramidal cells in the neocortex of control and *Cntnap2* mutant mice revealed no significant differences (Supplementary Fig. 2A–F). To confirm this observation, we carried out in utero electroporation experiments in which we labeled callosal layer 2/3 neurons with a plasmid encoding *Gfp* (Supplementary Fig. 2G). These experiments confirmed that pyramidal cell migration is not altered in the neocortex of *Cntnap2* mutants. In addition, we observed a similar organization of callosal axons in both genotypes (Supplementary Fig. 2H–K).

The previous results suggested that the differences in FV amplitudes between control and *Cntnap2* mutant mice are likely due to changes in the axonal action potential waveform and/or changes in fiber recruitment. To discriminate between these possibilities, we recorded single action potentials in loose-patch configuration by drawing individual

axons from the corpus callosum into suction electrodes. All-or-none action potentials were recorded after minimal stimulation from the contralateral corpus callosum. In this configuration, axonal deflections closely follow the first derivative of the action potential, where the peak corresponds to the maximal rise slope due to the opening of voltage-gated Na^+ conductances and the anti-peak corresponds to the maximal decay slope due to the opening of voltage gated K^+ conductances (Henze et al. 2000; Scott et al. 2014). We observed that anti-peak amplitudes are substantially reduced in 8 weeks old *Cntnap2* mutant mice compared to controls (Fig. 2D, E), a phenotype that is already apparent at 3 weeks of age (Fig. 2F, G). These results suggested that the improper distribution of Kv1-family channels in the axon slows down the repolarization phase of the action potential, thereby modifying the spike waveform in long-range myelinated axons.

Abnormal excitatory synaptic transmission in the neocortex of *Cntnap2* mutant mice

Changes in axonal action potential shape greatly alter neurotransmitter release (Sabatini and Regehr 1997) and these effects can be even passively transmitted at distal synaptic release sites (Alle and Geiger 2006; Shu et al. 2006). To evaluate the potential impact of the biophysical changes in action potential waveform observed in myelinated axons lacking Caspr2, we first recorded spontaneous excitatory postsynaptic currents (sEPSCs) from layer 2/3 pyramidal neurons in 8 weeks old mice. We observed that while the frequency of excitatory events recorded in these cells was similar for both genotypes (Fig. 3A, C), the mean amplitude of sEPSCs was significantly higher in pyramidal cells from *Cntnap2* mutant mice (Fig. 3A, D). Since this phenotype could be caused by a change in the number of excitatory synapses, we measured miniature events with whole-cell

recordings. Analysis of miniature excitatory postsynaptic currents (mEPSCs) showed no significant differences in the frequency and amplitude of synaptic events in pyramidal cells of *Cntnap2* mutant mice compared to controls (Supplementary Fig. 3A, C, D). Consequently, the abnormal rise in sEPSCs amplitude is likely linked to increased neurotransmitter release due to wider axonal action potentials in the myelinated presynaptic excitatory neurons.

Next we recorded evoked excitatory responses (eEPSCs) from layer 2/3 pyramidal cells following stimulation in the corpus callosum (Fig. 3G). Following the first stimulus, we observed a significant increase in the amplitude of eEPSCs in pyramidal cells from *Cntnap2* mutants compared to controls (Fig. 3H, I). Moreover, we found a prominent decrease in the paired-pulse ratio (PPR) when paired stimuli were applied as part of the stimulation protocol (Fig. 3J, J), indicating a reduced probability of release from these synapses in *Cntnap2* mutants during the second stimulus. These results strongly supported the notion that excitatory synaptic transmission is abnormally enhanced in the absence of Caspr2. Finally, to confirm that this phenotype is caused by the abnormally high release of excitatory terminals in *Cntnap2* mutant mice, we performed another series of experiments in which the concentration of extracellular calcium was reduced to 1 mM to decrease the probability of neurotransmitter release. We found that PPR differences between both genotypes are neutralized under these conditions (Fig. 3K, L), which reinforced the idea that an increase in release probability at excitatory neurons causes the abnormally high amplitude of excitatory responses observed in pyramidal cells from *Cntnap2* mutants.

Previous studies have reported deficits in the number of cortical interneurons in early postnatal *Cntnap2* mutant mice (Peñagarikano et al. 2011). To test the possible involvement of inhibition in the abnormally high amplitude of excitatory responses

observed in *Cntnap2* mutant mice, we investigated the extent of interneuron deficits in 8 weeks old mice. We recorded spontaneous inhibitory postsynaptic currents (sIPSCs) from layer 2/3 pyramidal neurons in 8 weeks old mice and found no changes in either the frequency or amplitude of sIPSCs (Fig. 3B, E, F). Consistent with this observation, we found no significant differences in the density and laminar distribution of cortical interneurons in the somatosensory cortex of *Cntnap2* mutant mice compared to controls (Fig. 4). Similarly, the distribution of hippocampal interneurons was comparable between both genotypes (data not shown). To extend these observations, we analyzed miniature inhibitory postsynaptic currents (mIPSCs) with whole-cell recordings from pyramidal cells and found no significant differences in the frequency and amplitude of synaptic events in pyramidal cells of *Cntnap2* mutant mice compared to controls (Supplementary Fig. 3B, E, F). Altogether, these observations revealed that inhibitory connectivity is normal in the neocortex of young adult *Cntnap2* mutant mice.

Delayed grey matter myelination in *Cntnap2* mutant mice

The previous results suggested that defects in excitatory neurotransmission are characteristic in *Cntnap2* mutant mice. We reasoned that a critical factor for the expressivity of the axonal action potential waveform phenotype observed in *Cntnap2* mutant mice is myelination, since only axons that are fully myelinated would maximally benefit from the clustered organization of potassium channels at the nodes of Ranvier. Interestingly, we found a significant reduction in grey matter myelination of the neocortex in juvenile *Cntnap2* mutant mice (Fig. 5A–C, F–H). In particular, while myelinated fibers have a comparable density in the corpus callosum and infragranular layers of the cortex in controls and *Cntnap2* mutants, the density of myelinated axons in superficial layers of the

neocortex was decreased in the absence of Caspr2 (Fig. 5C, E, H). Consistent with this observation, we found a significant reduction in the density of Sox10+ cells in the neocortex of 3 weeks old *Cntnap2* mutants compared to control mice (Fig. 5D, I, J).

The reduced myelination in the neocortex of juvenile *Cntnap2* mutant mice was also obvious in electrophysiological recordings measuring the speed of propagation of axon potentials. In these experiments, we stimulated the corpus callosum and recorded the local field potential (LFP) at progressively more distant sites, within the corpus callosum and also in the grey matter, while synaptic transmission was completely blocked with specific drugs (Fig. 5K). In these conditions, the LFP reflected mostly the action potentials propagating through the stimulated axons (Swadlow 1974). As suggested by the myelin staining, we found no differences in the speed of the action potentials propagating within the corpus callosum (up to 3000 μm from the stimulating electrode; Fig. 5L, M) between both genotypes. However, the speed of propagation was on average significantly slower in *Cntnap2* mutants than in control mice when the recordings were made within the grey matter (3000-6000 μm from the stimulating electrode; Fig. 5L, M), consistent with the reduction in the density of myelinated fibers observed in these mice. In particular, axons with fast propagation speeds (i.e., highly myelinated) were nearly absent from the recordings in *Cntnap2* mutants.

To distinguish whether the defects in myelination were transitory or permanent, we repeated these analyses in a cohort of 8 weeks old mice. We observed a recovery in the myelination of the neocortex in *Cntnap2* mutants: the density of myelinated fibers, number of Sox10+ cells, and propagation speeds were comparable between both genotypes (Supplementary Fig. 4). These results suggested that myelination is only transiently compromised in the neocortex of *Cntnap2* mutant mice.

Developmental onset of repetitive behaviors *Cntnap2* mutant mice

Given the wide implication of Caspr2 disruption in developmental disorders, we investigated the behavior of *Cntnap2* mutant mice using longitudinal assessment across postnatal developmental stages (Supplementary Fig. 1). At 4 weeks, we found no significant differences in the assessment of *Cntnap2* mutant mice compared to littermate wild type controls (Fig. 6A–C). From 6 weeks of age, significant behavioral abnormalities were found in *Cntnap2* mutants compared to control mice. Exposed to a novel empty cage, we observed increased repetitive behaviors in *Cntnap2* mutant mice that persisted into adulthood. These include increased grooming behavior and two previously unrecognized stereotyped motor phenotypes. One novel behavior was found in the grooming sequence; distinct episodes were identified when the ears were groomed alternately and repeatedly. We classified this behavior as rubbing. A second novel behavioral phenotype was identified as sudden non-rhythmic jerk-like movements of the whole body or body parts, further referred to as involuntary movements or tic-like behavior (Fig. 6A–D). In contrast, no differences were observed in rearing behavior (Supplementary Fig. 5A) or motor activity levels (data not shown) across the different developmental stages.

To establish whether these stereotyped motor behaviors might be due to reduced sensorimotor coordination, we examined motor balance and sensorimotor competence using the accelerating rotarod. We found no differences in performance between controls and littermate *Cntnap2* mutant mice at any of the ages examined (Supplementary Fig. 5B). In addition, *Cntnap2* mutants exhibited no alteration in reflexes, muscle strength, and sensory responses across the developmental stages (Supplementary Table 2), while a modest reduction in body and brain weights compared to controls was found (Supplementary Fig. 6A, B).

At adult age, we tested a multi-trial compound set-shifting paradigm and found no evidence that the repetitive behaviors in *Cntnap2* mutants were associated with cognitive inflexibility (Supplementary Fig. 7A). Subsequently, we used the home cage for unbiased monitoring of basic behavioral readouts. Assessment of feeding behavior indicated that *Cntnap2* mutant mice have similar levels of food intake, but duration of intake was reduced (Supplementary Fig. 6C, D). *Cntnap2* mutant mice displayed locomotor hyperactivity mainly when exposed to the home cage for the first time (Fig. 6F) and during the light phase, the habitual sleep phase for this nocturnal species (Fig. 6E and Supplementary Fig. 5C). In contrast, overall distance moved in the home cage was similar between control and *Cntnap2* mutant mice during the dark phase, the habitual activity phase (Fig. 6E and Supplementary Fig. 5C). Increased motor activity levels were also found when exposed to the elevated plus maze (Supplementary Fig. 5D). This activity in *Cntnap2* mutant mice compared to controls was restricted to the open arms of the maze (Supplementary Fig. 5E). This finding could suggest reduced anxiety-like behaviors in the absence of *Cntnap2*, which was contradicted by similar levels of inner and outer zone activity in the open field test (Supplementary Fig. 5F, G).

Finally, we tested the social behavioral domain and found that *Cntnap2* mutant mice showed similar levels of social interaction with genotype-matched conspecifics in a juvenile P21 social behavior test compared to controls. During this test, increased rubbing in the *Cntnap2* mutant mice was already evident (Supplementary Fig. 7B). At adult age, sociability in the standard three-chamber paradigm task, defined as spending more time with the novel mouse than with the novel object, were similar for control and *Cntnap2* mutant mice (Supplementary Fig. 7C). Social recognition memory in a direct social interaction test was also unmarked in both groups. Mice from both genotypes spent more

time sniffing a novel than a familiar mouse (Supplementary Fig. 7D). These data suggest that *Cntnap2* mutant mice do not have aberrant development of social interaction behavior.

Discussion

Our results indicate that loss of Caspr2 modifies the action potential waveform in central myelinated axons and causes an abnormal increase in neurotransmitter release. In the neocortex, for instance, loss of Caspr2 leads to increased postsynaptic excitatory responses in pyramidal cells. Our data suggest that the axonal biophysical changes observed in *Cntnap2* mutants are likely due to the abnormal clustering of Kv1-family potassium channels in the juxtaparanodes region of the nodes of Ranvier, a phenotype whose expressivity is linked to myelination. Consequently, relatively subtle defects in functional connectivity are likely widespread among central myelinated axons in *Cntnap2* mutants, and may contribute to the developmental trajectory of behavioral deficits here established for *Cntnap2* mutants. Our results reveal a pervasive mechanism through which CNTNAP2 mutations may predispose to neurodevelopmental conditions in humans.

Abnormal neurotransmitter release in *Cntnap2* mutant myelinated axons

Synaptic transmission can be modulated by electrotonic propagation of subthreshold membrane depolarization along axons (Alle and Geiger 2006; Shu et al. 2006). Previous studies have shown that depolarization-mediated inactivation of axonal Kv1-family potassium channels contribute to this form of "analog" signaling by broadening action potentials (Kole et al. 2007; Shu et al. 2007). Moreover, recent experiments using ion conductance microscopy have demonstrated that pharmacological inhibition and genetic deletion of Kv1.1 channels broadens presynaptic spikes at intact axonal boutons (Vivekananda et al. 2017). Consistently, we observed that defective clustering of Kv1 channels in myelinated axons of *Cntnap2* mutants modifies the shape of presynaptic action potentials. As previously shown in other central synapses, presynaptic spike broadening

leads to a proportional increase in Ca^{2+} influx (Geiger and Jonas 2000; Begum et al. 2016). Consequently, the functional consequence of the defective clustering of Kv1 channels in central myelinated axons is an abnormal increase in neurotransmitter release. In the neocortex, these defects translate into increased excitatory synaptic input onto pyramidal cells, as revealed by the higher amplitude of EPSCs observed in layer 2/3 pyramidal cells. Since the defects found in the clustering of Kv1 channels are likely present in all myelinated neurons, the abnormal increase in synaptic responses are probably present in other brain areas. It is conceivable, for instance, that pyramidal cells in layer 5 may also elicit increased excitatory responses in the striatum and other subcortical targets. Although *Cntnap2* mutants do not display overt seizures, it is possible that the defects in excitatory neurotransmission described here might be related to the abnormal increase in asymptomatic seizure-like spiking events observed in the cortex of *Cntnap2* mutants during EEG recordings (Thomas et al. 2016).

Previous work described a significant reduction in the number of cortical inhibitory neurons as the most likely cause underlying the behavioral defects observed in *Cntnap2* mutant mice (Peñagarikano et al. 2011). Our results, however, suggest that neocortical inhibitory circuits are grossly normal in developing and adult *Cntnap2* mutants. These results are consistent with the observations that juvenile and young adult *Cntnap2* mutant mice do not exhibit seizures during behavioral testing (Brunner et al. 2015; Thomas et al. 2016). It should be noted, however, that deficits in inhibitory synaptic transmission has been reported in the hippocampus of *Cntnap2* mutant mice (Jurgensen and Castillo 2015). Therefore, it is possible that the functional consequences of disrupting Caspr2 function may vary among different cortical areas.

Our results also suggest that the laminar distribution of neocortical pyramidal cells is apparently normal in *Cntnap2* mutants. Cortical dysplasia was reported in a previous analysis of *Cntnap2* mutants (Peñagarikano et al. 2011) and in the original description of patients carrying homozygous deletions in the *CNTNAP2* locus (Strauss et al. 2006). It is worth noting, however, that cortical dysplasia is not present in all patients carrying bi-allelic *CNTNAP2* mutations, even with a similar clinical picture (Smogavec et al. 2016). Consequently, cortical dysplasia might not be as common in CNTNAP2-related disorders as assumed previously. In addition, we found no obvious defects in the connectivity of layer 2/3 pyramidal cells, in contrast to previous reports (Anderson et al. 2012; Gdalyahu et al. 2015). One possibility is that the loss of Caspr2 in vivo impacts differentially the connectivity of pyramidal cells in different layers and regions of the neocortex, since the loss of dendritic spines has been reported for layer 5 pyramidal cells (Gdalyahu et al. 2015) and our analysis was restricted to layer 2/3 neurons.

Cortical myelination defects in *Cntnap2* mutant mice

Myelin plays a critical role enabling neuronal function, and defects in myelination have been linked to multiple neurological and neuropsychiatric disorders (Nave 2010). Our observations indicate that myelination is delayed in the neocortex of *Cntnap2* mutant mice, most probably due to an early deficit in the number of oligodendrocytes that seems to be compensated in the adult cortex. Although the precise mechanisms underlying this phenotype remain to be investigated, it is well established that the proliferation of oligodendrocyte precursor cells depends on the electrical activity of axons (Barres and Raff 1993).

Resting state fMRI studies in mice suggest that white-matter connectivity is normal in adult *Cntnap2* mutant mice (Liska et al. 2017), which is consistent with our histological and electrophysiological observations at 8 weeks. However, the reduced myelination observed in juvenile *Cntnap2* mutant mice is likely responsible for the absence of fast propagation speeds observed at this stage. This phenotype, during a critical developmental window, may influence network dynamics of cortical neurons and perturb the consolidation of long-range functional connectivity (Wang et al. 2008), as previously described in ASD (Vissers et al. 2012; Rane et al. 2015). Recent imaging studies in humans have also reported transient defects in the corpus callosum of young toddlers later diagnosed with ASD (Wolff et al. 2015; Fingher et al. 2017), prior to the onset of behavioral abnormalities.

Expressivity of neurodevelopmental phenotypes in *Cntnap2* mutant mice

Our experiments revealed defects in the waveform of axonal action potentials in *Cntnap2* mutant mice at 3 weeks of age, prior to the onset of behavioral abnormalities. There are two possible, non-exclusive explanations for this divergence. Firstly, the characteristic organization of channels at the nodes of Ranvier, which likely underlies the changes in the waveform of axonal action potentials observed in *Cntnap2* mutants, is directly linked to the process of myelination. Indeed, channels cluster progressively in their mature location in parallel to the process of myelination (Rasband et al. 1999; Vabnick et al. 1999), and so their impact on axonal physiology increases with age under normal circumstances. Since myelination is delayed in *Cntnap2* mutants, the relatively late onset of behavioral phenotypes may indicate that the consequences of the changes in axonal physiology may only manifest fully when myelination is completed.

Secondly, clinical research and experimental manipulations in rodents suggest a role for abnormal function of cortico-striatal-thalamo-cortical circuits in repetitive motor behaviors (Saxena et al. 1998; Marsh et al. 2009; Ahmari et al. 2013; Burguiere et al. 2013). The nature of the stereotyped motor behaviors observed in *Cntnap2* mutants reflects inadequate coping and arousal in response to unexpected or novel situations (Turner 1999; Richler et al. 2007; Geurts et al. 2009; Lewis and Kim 2009), which is consistent with a role of cortico-striatal circuits independently of a more complex set of mental operations involved in cognitive flexibility and social interactions (Geurts et al. 2009). Interestingly, repeated – but not acute – optogenetic hyperactivation of cortico-striatal connections over multiple days generates a progressive increase in grooming in mice (Ahmari et al. 2013). Thus, it is conceivable that a sustained increase in postsynaptic responses at cortico-striatal synapses during early postnatal development may lead to the motor stereotypies characteristic of *Cntnap2* mutant mice, although this hypothesis remains to be experimentally tested.

Acknowledgements

We thank C. Serra for excellent technical assistance, T. Gil and M. Fernández-Otero for lab support, M. N. Rasband and M. Wegner for antibodies, and J. L. R. Rubenstein for plasmids. We are grateful to J. Burrone for critical reading of the manuscript, and members of the Marín and Rico laboratories for stimulating discussions and ideas. This work was supported by grants from the Spanish Ministerio de Economía (SAF2010-20604) to R.S.; Israel Science Foundation to E.P.; Simons Foundation (SFARI 239766) to E.P. and O.M.; the European Research Council (ERC-2011-AdG 293683) to O.M.; and the European Autism Interventions – A Multicentre Study for Developing New Medications (EU-AIMS) to M.K. EU-AIMS is a project receiving support from the Innovative Medicines Initiative Joint Undertaking under grant agreement n° 115300, resources of which are composed of financial contribution from the European Union's Seventh Framework Programme (FP7/2007-2013), from the EFPIA companies in kind contribution, and from Autism Speaks. O.M. is a Wellcome Trust Investigator. The authors report no financial interests or potential conflicts of interest.

References

Ahmari SE, Spellman T, Douglass NL, Kheirbek MA, Simpson HB, Deisseroth K, Gordon JA, Hen R. 2013. Repeated cortico-striatal stimulation generates persistent OCD-like behavior. Science 340:1234-1239.

Alle H, Geiger JR. 2006. Combined analog and action potential coding in hippocampal mossy fibers. Science 311:1290-1293.

Anderson GR, Galfin T, Xu W, Aoto J, Malenka RC, Sudhof TC. 2012. Candidate autism gene screen identifies critical role for cell-adhesion molecule CASPR2 in dendritic arborization and spine development. Proc Natl Acad Sci USA 109:18120-18125.

Barres BA, Raff MC. 1993. Proliferation of oligodendrocyte precursor cells depends on electrical activity in axons. Nature 361:258-260.

Begum R, Bakiri Y, Volynski KE, Kullmann DM. 2016. Action potential broadening in a presynaptic channelopathy. Nat Commun 7:12102.

Brunner D, Kabitzke P, He D, Cox K, Thiede L, Hanania T, Sabath E, Alexandrov V, Saxe M, Peles E, et al. 2015. Comprehensive Analysis of the 16p11.2 Deletion and Null Cntnap2 Mouse Models of Autism Spectrum Disorder. PLoS One 10:e0134572.

Burguiere E, Monteiro P, Feng G, Graybiel AM. 2013. Optogenetic stimulation of lateral orbitofronto-striatal pathway suppresses compulsive behaviors. Science 340:1243-1246.

Centanni TM, Sanmann JN, Green JR, Iuzzini-Seigel J, Bartlett C, Sanger WG, Hogan TP. 2015. The role of candidate-gene CNTNAP2 in childhood apraxia of speech and specific language impairment. Am J Med Genet B Neuropsychiatr Genet 168:536-543.

Cross-Disorder Group of the Psychiatric Genomics C, Lee SH, Ripke S, Neale BM, Faraone SV, Purcell SM, Perlis RH, Mowry BJ, Thapar A, Goddard ME, et al. 2013. Genetic relationship between five psychiatric disorders estimated from genome-wide SNPs. Nat Genet 45:984-994.

De Rubeis S, He X, Goldberg AP, Poultney CS, Samocha K, Cicek AE, Kou Y, Liu L, Fromer M, Walker S, et al. 2014. Synaptic, transcriptional and chromatin genes disrupted in autism. Nature 515:209-215.

Dennis EL, Jahanshad N, Rudie JD, Brown JA, Johnson K, McMahon KL, de Zubicaray GI, Montgomery G, Martin NG, Wright MJ, et al. 2011. Altered structural brain connectivity in healthy carriers of the autism risk gene, CNTNAP2. Brain Connect 1:447-459.

Fingher N, Dinstein I, Ben-Shachar M, Haar S, Dale AM, Eyler L, Pierce K, Courchesne E. 2017. Toddlers later diagnosed with autism exhibit multiple structural abnormalities in temporal corpus callosum fibers. Cortex doi: 10.1016/j.cortex.2016.12.024.

Friedman JI, Vrijenhoek T, Markx S, Janssen IM, van der Vliet WA, Faas BH, Knoers NV, Cahn W, Kahn RS, Edelmann L, et al. 2008. CNTNAP2 gene dosage variation is associated with schizophrenia and epilepsy. Mol Psychiatry 13:261-266.

Fromer M, Pocklington AJ, Kavanagh DH, Williams HJ, Dwyer S, Gormley P, Georgieva L, Rees E, Palta P, Ruderfer DM, et al. 2014. De novo mutations in schizophrenia implicate synaptic networks. Nature 506:179-184.

Gdalyahu A, Lazaro M, Penagarikano O, Golshani P, Trachtenberg JT, Geschwind DH. 2015. The Autism Related Protein Contactin-Associated Protein-Like 2 (CNTNAP2) Stabilizes New Spines: An In Vivo Mouse Study. PLoS One 10:e0125633.

Geiger JR, Jonas P. 2000. Dynamic control of presynaptic Ca(2+) inflow by fast-inactivating K(+) channels in hippocampal mossy fiber boutons. Neuron 28:927-939.

Geurts HM, Corbett B, Solomon M. 2009. The paradox of cognitive flexibility in autism. Trends Cogn Sci 13:74-82.

Gordon A, Salomon D, Barak N, Pen Y, Tsoory M, Kimchi T, Peles E. 2016. Expression of Cntnap2 (Caspr2) in multiple levels of sensory systems. Mol Cell Neurosci 70:42-53.

Guilmatre A, Huguet G, Delorme R, Bourgeron T. 2014. The emerging role of SHANK genes in neuropsychiatric disorders. Dev Neurobiol 74:113-122.

Henze DA, Borhegyi Z, Csicsvari J, Mamiya A, Harris KD, Buzsaki G. 2000. Intracellular features predicted by extracellular recordings in the hippocampus in vivo. J Neurophysiol 84:390-400.

Hoffman EJ, Turner KJ, Fernandez JM, Cifuentes D, Ghosh M, Ijaz S, Jain RA, Kubo F, Bill BR, Baier H, et al. 2016. Estrogens Suppress a Behavioral Phenotype in Zebrafish Mutants of the Autism Risk Gene, CNTNAP2. Neuron 89:725-733.

Inda MC, DeFelipe J, Munoz A. 2006. Voltage-gated ion channels in the axon initial segment of human cortical pyramidal cells and their relationship with chandelier cells. Proc Natl Acad Sci U S A 103:2920-2925.

Jurgensen S, Castillo PE. 2015. Selective Dysregulation of Hippocampal Inhibition in the Mouse Lacking Autism Candidate Gene CNTNAP2. J Neurosci 35:14681-14687.

Kole MH, Letzkus JJ, Stuart GJ. 2007. Axon initial segment Kv1 channels control axonal action potential waveform and synaptic efficacy. Neuron 55:633-647.

Kumar SS, Huguenard JR. 2001. Properties of excitatory synaptic connections mediated by the corpus callosum in the developing rat neocortex. J Neurophysiol 86:2973-2985.

Lewis M, Kim SJ. 2009. The pathophysiology of restricted repetitive behavior. J Neurodev Disord 1:114-132.

Liska A, Bertero A, Gomolka R, Sabbioni M, Galbusera A, Barsotti N, Panzeri S, Scattoni ML, Pasqualetti M, Gozzi A. 2017. Homozygous loss of autism-risk gene CNTNAP2 results in reduced local and long-range prefrontal functional connectivity. Cereb Cortex 10.1093/cercor/bhx022.

Marsh R, Maia TV, Peterson BS. 2009. Functional disturbances within frontostriatal circuits across multiple childhood psychopathologies. Am J Psychiatry 166:664-674.

McCarthy SE, Gillis J, Kramer M, Lihm J, Yoon S, Berstein Y, Mistry M, Pavlidis P, Solomon R, Ghiban E, et al. 2014. De novo mutations in schizophrenia implicate chromatin remodeling and support a genetic overlap with autism and intellectual disability. Mol Psychiatry 19:652-658.

Nave KA. 2010. Myelination and support of axonal integrity by glia. Nature 468:244-252.

Ogawa Y, Horresh I, Trimmer JS, Bredt DS, Peles E, Rasband MN. 2008. Postsynaptic density-93 clusters Kv1 channels at axon initial segments independently of Caspr2. J Neurosci 28:5731-5739.

Peñagarikano O, Abrahams BS, Herman EI, Winden KD, Gdalyahu A, Dong H, Sonnenblick LI, Gruver R, Almajano J, Bragin A, et al. 2011. Absence of CNTNAP2 leads to epilepsy, neuronal migration abnormalities, and core autism-related deficits. Cell 147:235-246.

Pla R, Borrell V, Flames N, Marín O. 2006. Layer acquisition by cortical GABAergic interneurons is independent of Reelin signaling. J Neurosci 26:6924-6934.

Poliak S, Gollan L, Martinez R, Custer A, Einheber S, Salzer JL, Trimmer JS, Shrager P, Peles E. 1999. Caspr2, a new member of the neurexin superfamily, is localized at the

juxtaparanodes of myelinated axons and associates with K+ channels. Neuron 24:1037-1047.

Poliak S, Gollan L, Salomon D, Berglund EO, Ohara R, Ranscht B, Peles E. 2001. Localization of Caspr2 in myelinated nerves depends on axon-glia interactions and the generation of barriers along the axon. J Neurosci 21:7568-7575.

Poliak S, Salomon D, Elhanany H, Sabanay H, Kiernan B, Pevny L, Stewart CL, Xu X, Chiu SY, Shrager P, et al. 2003. Juxtaparanodal clustering of Shaker-like K+ channels in myelinated axons depends on Caspr2 and TAG-1. J Cell Biol 162:1149-1160.

Poot M. 2015. Connecting the CNTNAP2 networks with neurodevelopmental disorders. Mol Syndromol 6:7-22.

Rane P, Cochran D, Hodge SM, Haselgrove C, Kennedy DN, Frazier JA. 2015. Connectivity in Autism: A Review of MRI Connectivity Studies. Harv Rev Psychiatry 23:223-244.

Rasband MN, Trimmer JS, Peles E, Levinson SR, Shrager P. 1999. K+ channel distribution and clustering in developing and hypomyelinated axons of the optic nerve. J Neurocytol 28:319-331.

Richler J, Bishop SL, Kleinke JR, Lord C. 2007. Restricted and repetitive behaviors in young children with autism spectrum disorders. J Autism Dev Disord 37:73-85.

Rodenas-Cuadrado P, Ho J, Vernes SC. 2014. Shining a light on CNTNAP2: complex functions to complex disorders. Eur J Hum Genet 22:171-178.

Sabatini BL, Regehr WG. 1997. Control of neurotransmitter release by presynaptic waveform at the granule cell to Purkinje cell synapse. J Neurosci 17:3425-3435.

Saxena S, Brody AL, Schwartz JM, Baxter LR. 1998. Neuroimaging and frontal-subcortical circuitry in obsessive-compulsive disorder. Br J Psychiatry Suppl:26-37.

Scott RS, Henneberger C, Padmashri R, Anders S, Jensen TP, Rusakov DA. 2014. Neuronal adaptation involves rapid expansion of the action potential initiation site. Nat Commun 5:3817.

Scott-Van Zeeland AA, Abrahams BS, Alvarez-Retuerto AI, Sonnenblick LI, Rudie JD, Ghahremani D, Mumford JA, Poldrack RA, Dapretto M, Geschwind DH, et al. 2010. Altered functional connectivity in frontal lobe circuits is associated with variation in the autism risk gene CNTNAP2. Science Transl Med 2:56ra80.

Shu Y, Hasenstaub A, Duque A, Yu Y, McCormick DA. 2006. Modulation of intracortical synaptic potentials by presynaptic somatic membrane potential. Nature 441:761-765.

Shu Y, Yu Y, Yang J, McCormick DA. 2007. Selective control of cortical axonal spikes by a slowly inactivating K+ current. Proc Natl Acad Sci USA 104:11453-11458.

Smogavec M, Cleall A, Hoyer J, Lederer D, Nassogne MC, Palmer EE, Deprez M, Benoit V, Maystadt I, Noakes C, et al. 2016. Eight further individuals with intellectual disability and epilepsy carrying bi-allelic CNTNAP2 aberrations allow delineation of the mutational and phenotypic spectrum. J Med Genet 53:820-827.

Strauss KA, Puffenberger EG, Huentelman MJ, Gottlieb S, Dobrin SE, Parod JM, Stephan DA, Morton DH. 2006. Recessive symptomatic focal epilepsy and mutant contactin-associated protein-like 2. New Engl J Med 354:1370-1377.

Swadlow HA. 1974. Properties of antidromically activated callosal neurons and neurons responsive to callosal input in rabbit binocular cortex. Exp Neurol 43:424-444.

Thomas AM, Schwartz MD, Saxe MD, Kilduff TS. 2016. Cntnap2 knockout rats and mice exhibit epileptiform activity and abnormal sleep/wake physiology. Sleep doi: 10.1093/sleep/zsw026.

Ting JT, Daigle TL, Chen Q, Feng G. 2014. Acute brain slice methods for adult and aging animals: application of targeted patch clamp analysis and optogenetics. Methods Mol Biol 1183:221-242.

Tomassy GS, Berger DR, Chen HH, Kasthuri N, Hayworth KJ, Vercelli A, Seung HS, Lichtman JW, Arlotta P. 2014. Distinct profiles of myelin distribution along single axons of pyramidal neurons in the neocortex. Science 344:319-324.

Traka M, Goutebroze L, Denisenko N, Bessa M, Nifli A, Havaki S, Iwakura Y, Fukamauchi F, Watanabe K, Soliven B, et al. 2003. Association of TAG-1 with Caspr2 is essential for the molecular organization of juxtaparanodal regions of myelinated fibers. J Cell Biol 162:1161-1172.

Turner M. 1999. Annotation: Repetitive behaviour in autism: a review of psychological research. J Child Psychol Psychiatry 40:839-849.

Vabnick I, Trimmer JS, Schwarz TL, Levinson SR, Risal D, Shrager P. 1999. Dynamic potassium channel distributions during axonal development prevent aberrant firing patterns. J Neurosci 19:747-758.

Varea O, Martin-de-Saavedra MD, Kopeikina KJ, Schurmann B, Fleming HJ, Fawcett-Patel JM, Bach A, Jang S, Peles E, Kim E, et al. 2015. Synaptic abnormalities and cytoplasmic glutamate receptor aggregates in contactin associated protein-like 2/Caspr2 knockout neurons. Proc Natl Acad Sci USA 112:6176-6181.

Vissers ME, Cohen MX, Geurts HM. 2012. Brain connectivity and high functioning autism: a promising path of research that needs refined models, methodological convergence, and stronger behavioral links. Neurosci Biobehav Rev 36:604-625.

Vivekananda U, Novak P, Bello OD, Korchev YE, Krishnakumar SS, Volynski KE, Kullmann DM. 2017. Kv1.1 channelopathy abolishes presynaptic spike width modulation by subthreshold somatic depolarization. Proc Natl Acad Sci USA.

Wang SS, Shultz JR, Burish MJ, Harrison KH, Hof PR, Towns LC, Wagers MW, Wyatt KD. 2008. Functional trade-offs in white matter axonal scaling. J Neurosci 28:4047-4056.

Wolff JJ, Gerig G, Lewis JD, Soda T, Styner MA, Vachet C, Botteron KN, Elison JT, Dager SR, Estes AM, et al. 2015. Altered corpus callosum morphology associated with autism over the first 2 years of life. Brain 138:2046-2058.

Worthey EA, Raca G, Laffin JJ, Wilk BM, Harris JM, Jakielski KJ, Dimmock DP, Strand EA, Shriberg LD. 2013. Whole-exome sequencing supports genetic heterogeneity in childhood apraxia of speech. J Neurodev Disord 5:29.

Zhou L, Zhang CL, Messing A, Chiu SY. 1998. Temperature-sensitive neuromuscular transmission in Kv1.1 null mice: role of potassium channels under the myelin sheath in young nerves. J Neurosci 18:7200-7215.

Zhou Y, Kaiser T, Monteiro P, Zhang X, Van der Goes MS, Wang D, Barak B, Zeng M, Li C, Lu C, et al. 2016. Mice with Shank3 mutations associated with ASD and schizophrenia display both shared and distinct defects. Neuron 89:147-162.

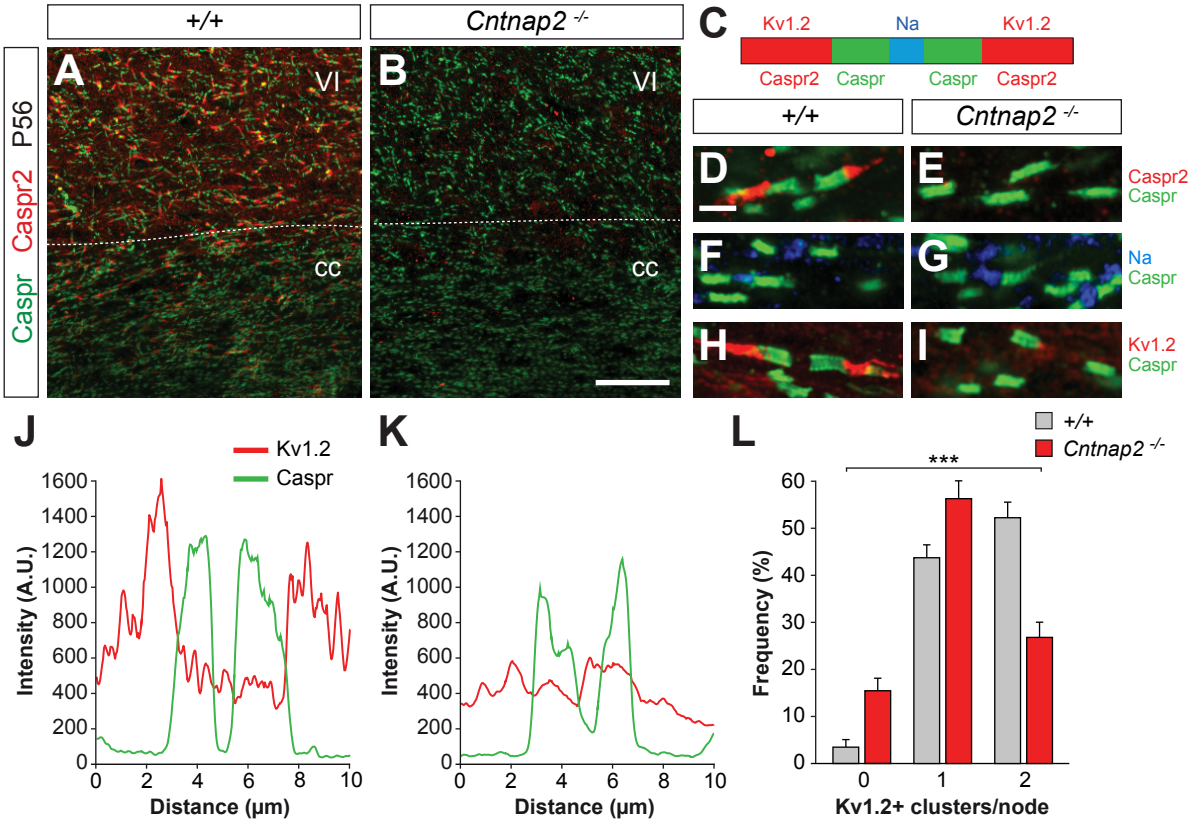

Figure 1. Abnormal clustering of Kv1.2 channels at the nodes of Ranvier in the telencephalon of *Cntnap2* mutant mice. (**A, B**) Caspr and Caspr2 expression in the corpus callosum (cc) and layer 6 of the neocortex in 8 weeks old control (A) and *Cntnap2* mutant (B) mice. (**C**) Schematic illustrating the normal distribution of proteins at the node (blue), paranodes (green) and juxtaparanodes (red). (**D–I**) High magnification images illustrating the expression of Caspr (green; D–I), Caspr2 (red; D, E), Na+ channels (blue; F, G) and Kv1.2 (red; H, I) channels at the node of Ranvier in corpus callosum axons from control (D, F, H) and *Cntnap2* mutant (E, G, I) mice. (**J, K**) Representative traces depicting relative levels of expression of Caspr and Kv1.2 at the paranode and juxtaparanode in control (J) and *Cntnap2* mutant (K) mice. These traces were used to determine the number of Caspr and Kv1.2 clusters present in each node. (**L**) Quantification of the relative frequency of nodes of Ranvier containing zero, one or two Kv1.2 clusters in control and *Cntnap2* mutant mice; $n = 263$ and 201 nodes from 3 control and 3 *Cntnap2* mutant mice, respectively; X2 test, $^{***}p = 0.001$. Histograms show average ± SEM. Scale bars equal 200 μm (A, B) and 10 μm (D–I).

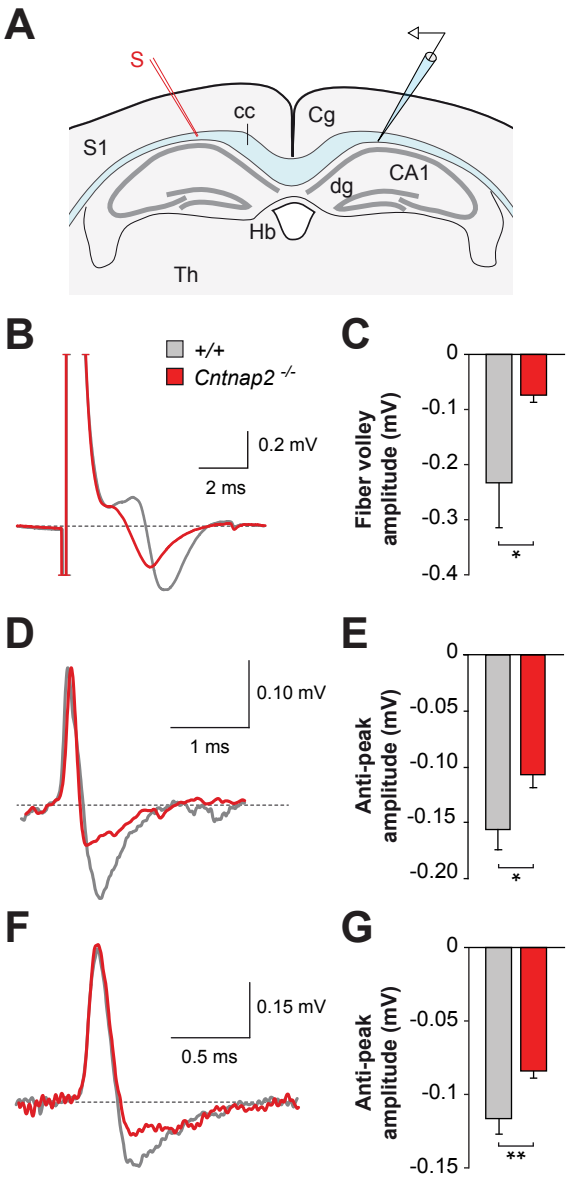

Figure 2. Action potential repolarization in cortical axons is altered in *Cntnap2* mutant mice. (**A**) Schematic of the experimental design. (**B**) Representative fiber volley traces from 8 weeks old control and *Cntnap2* mutant mice. Traces are the mean of 10 sweeps. The traces were subtracted after the application of TTX to reduce the stimulating artifact. (**C**) Quantification of fiber volley amplitudes. $n = 8$ FV from 8 control mice and 10 FV from 9 *Cntnap2* mutant mice; *t*-test, $^{*}p < 0.05$. (**D**) Representative traces of loose patch single axon potentials recorded in the corpus callosum of 8 weeks old control and *Cntnap2* mutant mice. (**E**) Quantification of anti-peak amplitudes; $n = 39$ axons from control mice and 39 axons from *Cntnap2* mutant mice; *t*-test, $^{*}p < 0.05$. (**F**) Representative traces of loose patch single axon potentials recorded in the corpus callosum of 3 weeks old control and *Cntnap2* mutant mice. (**G**) Quantification of anti-peak amplitudes; $n = 41$ axons from control mice and 44 axons from *Cntnap2* mutant mice; *t*-test, $^{**}p < 0.01$. Histograms show average ± SEM. CA1, CA1 region of the hippocampus; cc, corpus callosum; Cg, cingulate cortex; dg, dentate gyrus; Hb, habenula; S, stimulating electrode; S1, primary somatosensory cortex; Th, thalamus.

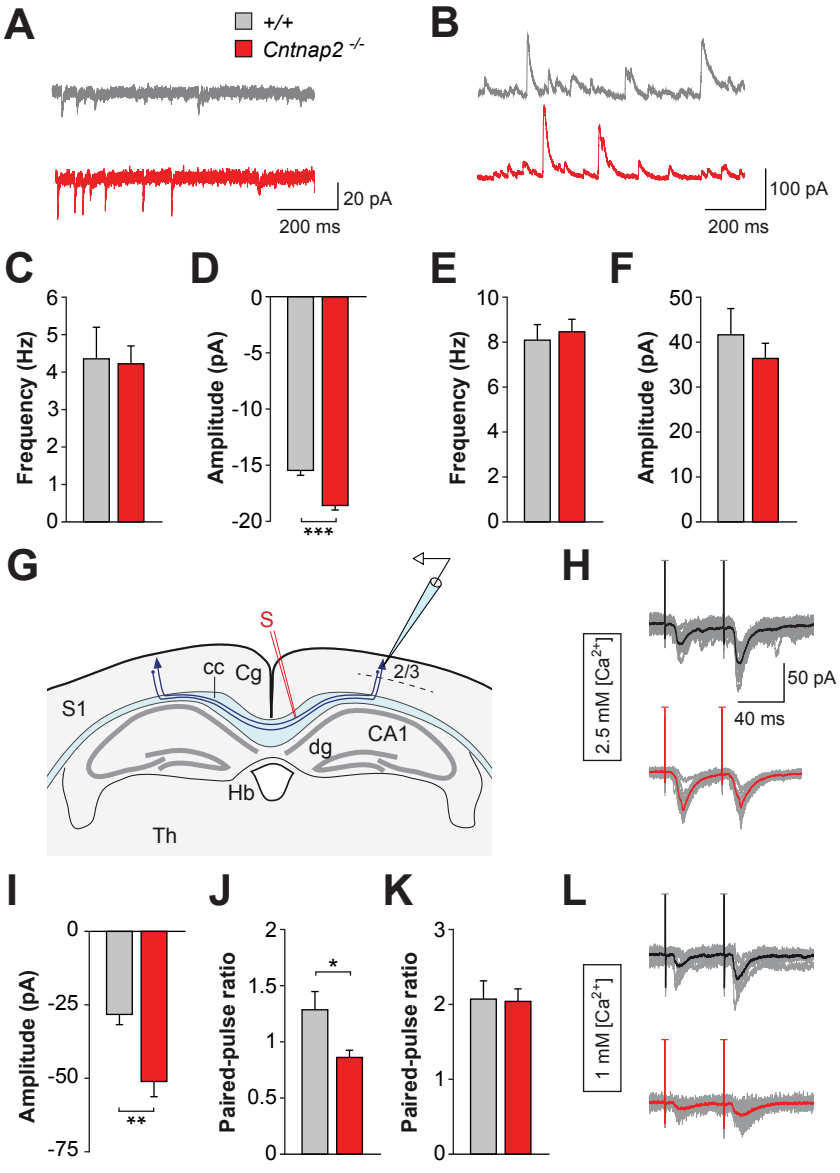

Figure 3. Abnormal excitatory synaptic transmission in the neocortex of *Cntnap2* mutant mice. (**A, B**) Representative traces of sEPSCs and sIPSCs recorded from layer 2/3 pyramidal neurons in control and *Cntnap2* mutant mice. (**C, D**) Quantification of sEPSCs frequencies (C) and amplitudes (D) in pyramidal cells; *n* = 13 and 18 cells in control and *Cntnap2* mutant mice, respectively; *t*-test, *p* = 0.56 (C) and *p < 0.001 (D). (**E, F**) Quantification of sIPSCs frequencies (E) and amplitudes (F) in pyramidal cells; *n* = 13 and 18 cells in control and *Cntnap2* mutant mice, respectively; *t*-test, *p* = 0.79 (E) and *p* = 0.46 (F). (**G**) Schematic of the experimental design. (**H, L**) Representative traces of eEPSCs recorded from layer 2/3 pyramidal neurons following paired pulses in control and *Cntnap2* mutant mice with 2.5 mM (H) and 1 mM (L) extracellular calcium. (**I**) Quantification of EPSCs amplitudes evoked in control and *Cntnap2* mutant mice; *n* = 18 and 17 cells in control and *Cntnap2* mutant mice, respectively; *t*-test, **p* < 0.01. (**J, K**) Quantification of paired-pulse ratios in control and *Cntnap2* mutant mice with 2.5 mM (J) and 1 mM (K) extracellular calcium; *n* = 14 and 13 cells in control and *Cntnap2* mutant mice, respectively; *t*-test, **p* < 0.05 (J) and p = 0.87 (K). Histograms show average ± SEM. CA1, CA1 region of the hippocampus; cc, corpus callosum; Cg, cingulate cortex; dg, dentate gyrus; Hb, habenula; S, stimulating electrode; S1, primary somatosensory cortex; Th, thalamus; 2/3, pyramidal cell in cortical layer 2/3.

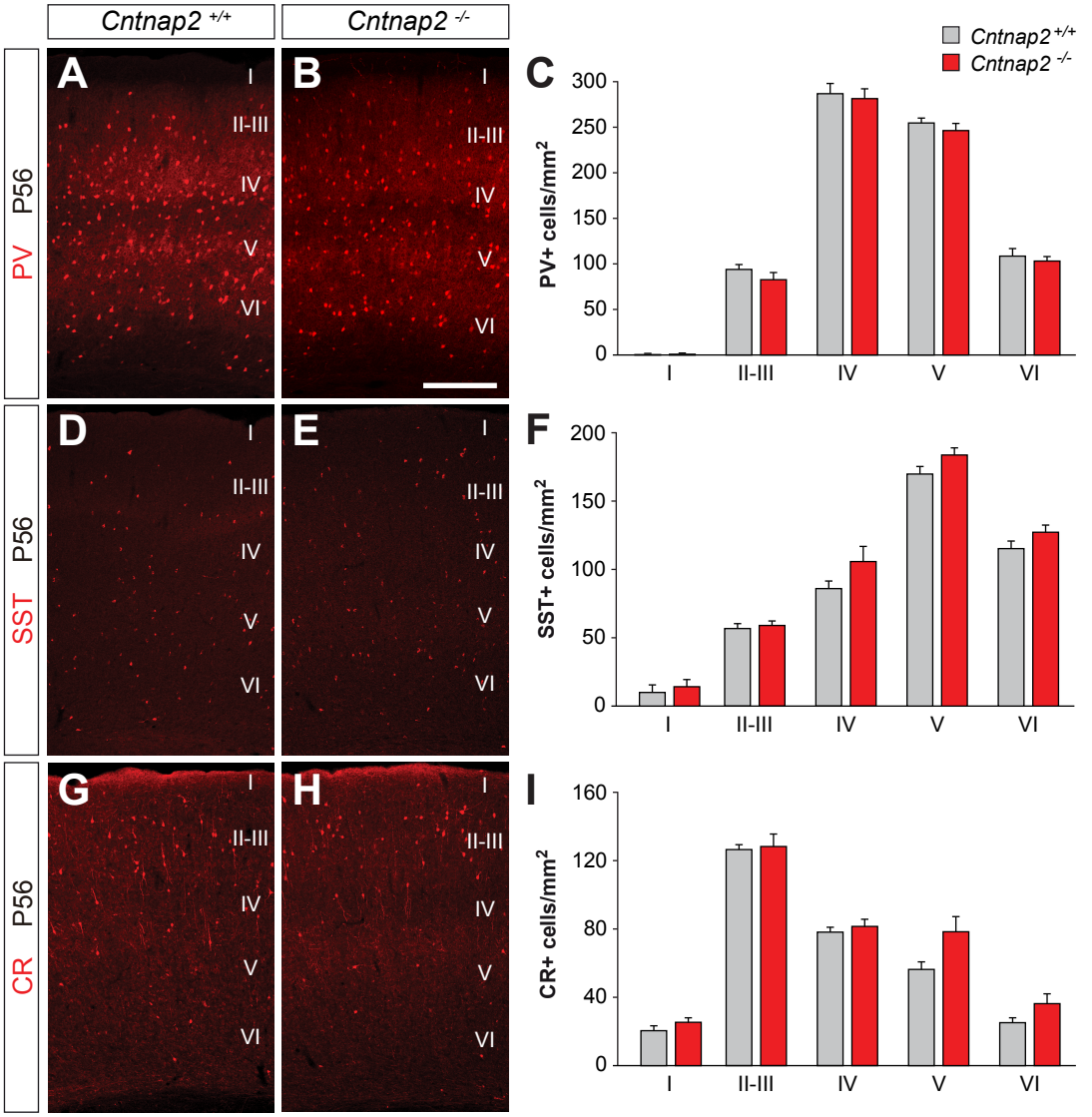

Figure 4. Normal distribution of cortical interneurons in the neocortex of adult *Cntnap2* mutant mice. (**A, B, D, E, G, H**) Distribution of PV+ (A, B), SST+ (D, E) and CR+ (G, H) interneurons in the somatosensory cortex of control (A, D, G) and *Cntnap2* mutant (B, E, H) mice. (**C, F, I**) Laminar distribution of PV+ (C), SST+ (F) and CR+ (I) interneurons; $n = 4$ control and *Cntnap2* mutant mice, two-way ANOVA, $p = 0.98$ (C), $p = 0.88$ (F) and $p = 0.78$ (I). Scale bar equals 200 µm.

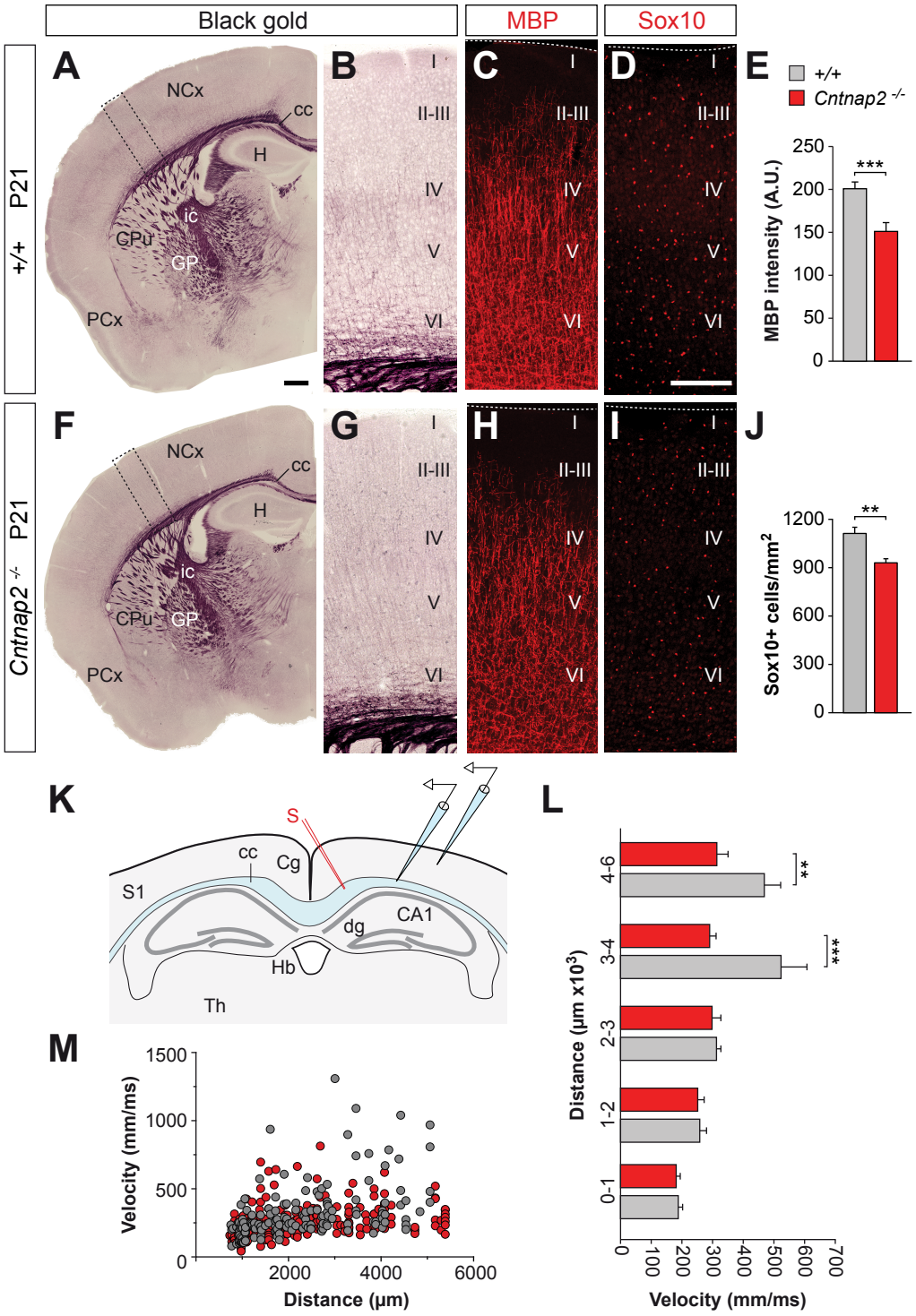

Figure 5. Delayed myelination of cortical grey matter in *Cntnap2* mutant mice. (**A–D, F–I**) Histological staining of myelin by Black gold (A, B, F, G) and immunohistochemistry for MBP (C, H) and Sox10 (D, I) in the neocortex of 3 weeks old control (A–D) and *Cntnap2* mutant (F–I) mice. (**E**) Quantification of MBP intensity in the somatosensory cortex; $n = 4$ control and 4 *Cntnap2* mutant mice, *t*-test, $^{***}p < 0.001$. (**J**) Quantification of the density of Sox10+ cells in the somatosensory cortex; $n = 4$ control and 4 *Cntnap2* mutant mice, *t*-test, $^{**}p < 0.01$. (**K**) Schematic of the experimental design. (**L**) Quantification of axonal conductance speeds as a function of distance. Bins under 3000 µm correspond to recordings within the corpus callosum, while bins over 3000 µm correspond to recordings within the cortical grey matter; $n = 152$ axons from control mice and 187 axons from *Cntnap2* mutant mice, two-way ANOVA, $^{**}p < 0.01$, $^{***}p < 0.001$. (**M**) Distribution of axonal conductance speed for individual axons at different distances from the stimulation electrode . Histograms show average ± SEM. CA1, CA1 region of the hippocampus; cc, corpus callosum; Cg, cingulate cortex; dg, dentate gyrus; Hb, habenula; S, stimulating electrode; S1, primary somatosensory cortex; Th, thalamus; 2/3, pyramidal cell in cortical layer 2/3. Scale bar equals 200 µm.

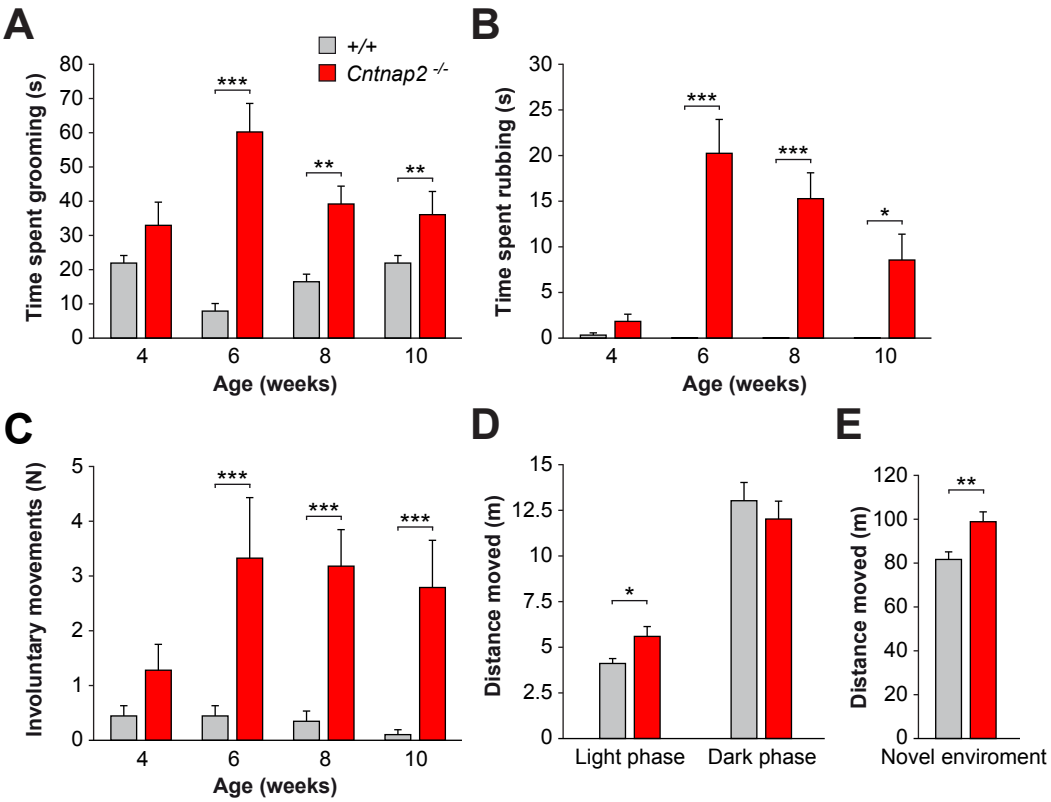

Figure 6. Developmental onset of motor abnormalities and repetitive behaviors in *Cntnap2* mutant mice. (**A–C**) Quantification of time spent grooming (A) or rubbing (B), and total amount of involuntary movements (C). (**D**) Quantification of distance moved in light and dark phase. (**E**) Quantification of activity for 1 hour in a novel environment. Histograms show average ± SEM. *n* = 11-14 control and 10-12 *Cntnap2* mutant mice; RM-ANOVA, **p* < 0.05, ***p* < 0.01, ****p* < 0.001.

Supplementary Information

Loss of *Cntnap2* causes axonal excitability deficits, developmental delay in cortical myelination, and abnormal stereotyped motor behavior

Ricardo Scott, Alberto Sánchez-Aguilera, Kim van Elst, Lynette Lim, Nathalie Dehorter, Sung Eun Bae, Giorgia Bartolini, Elior Peles, Martien J. H. Kas, Hilgo Bruining and Oscar Marín

Includes:

- Supplementary figures 1-7 and legends
- Supplementary tables 1 and 2
- Extended Methods and Materials

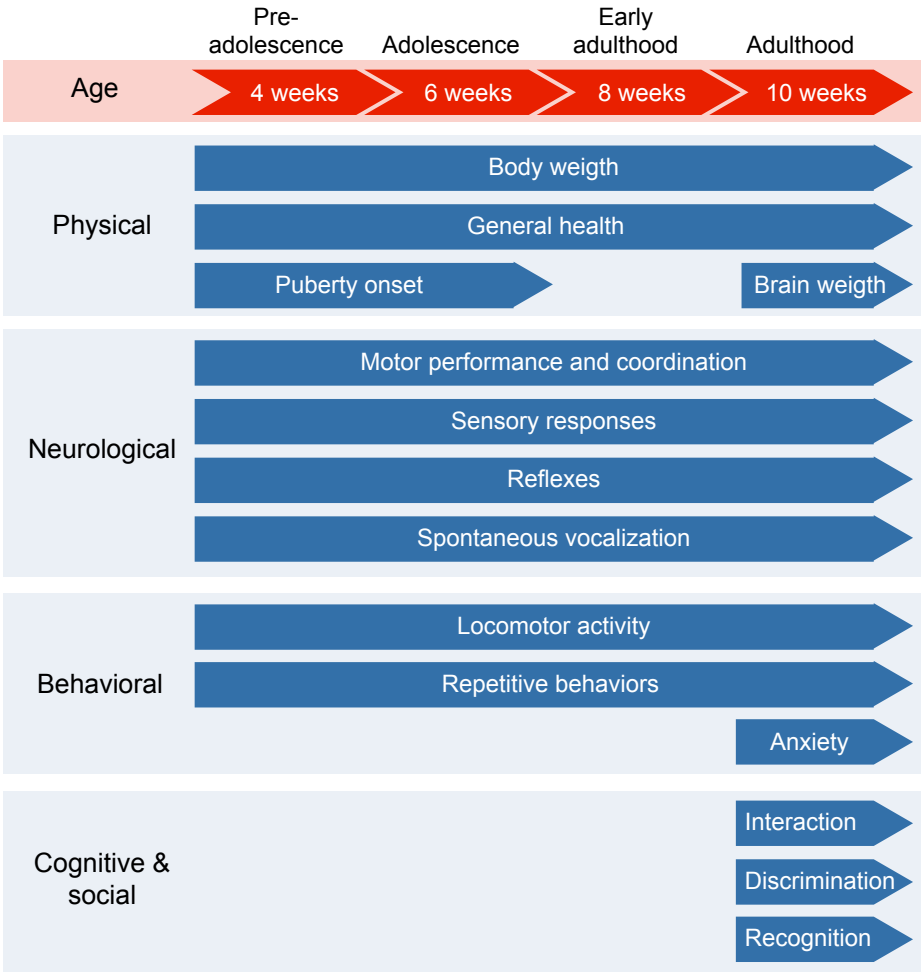

Supplementary Figure 1. Overview of all longitudinal tests and analyses performed to assess the developmental onset of behavioral abnormalities in *Cntnap2* mutant mice.

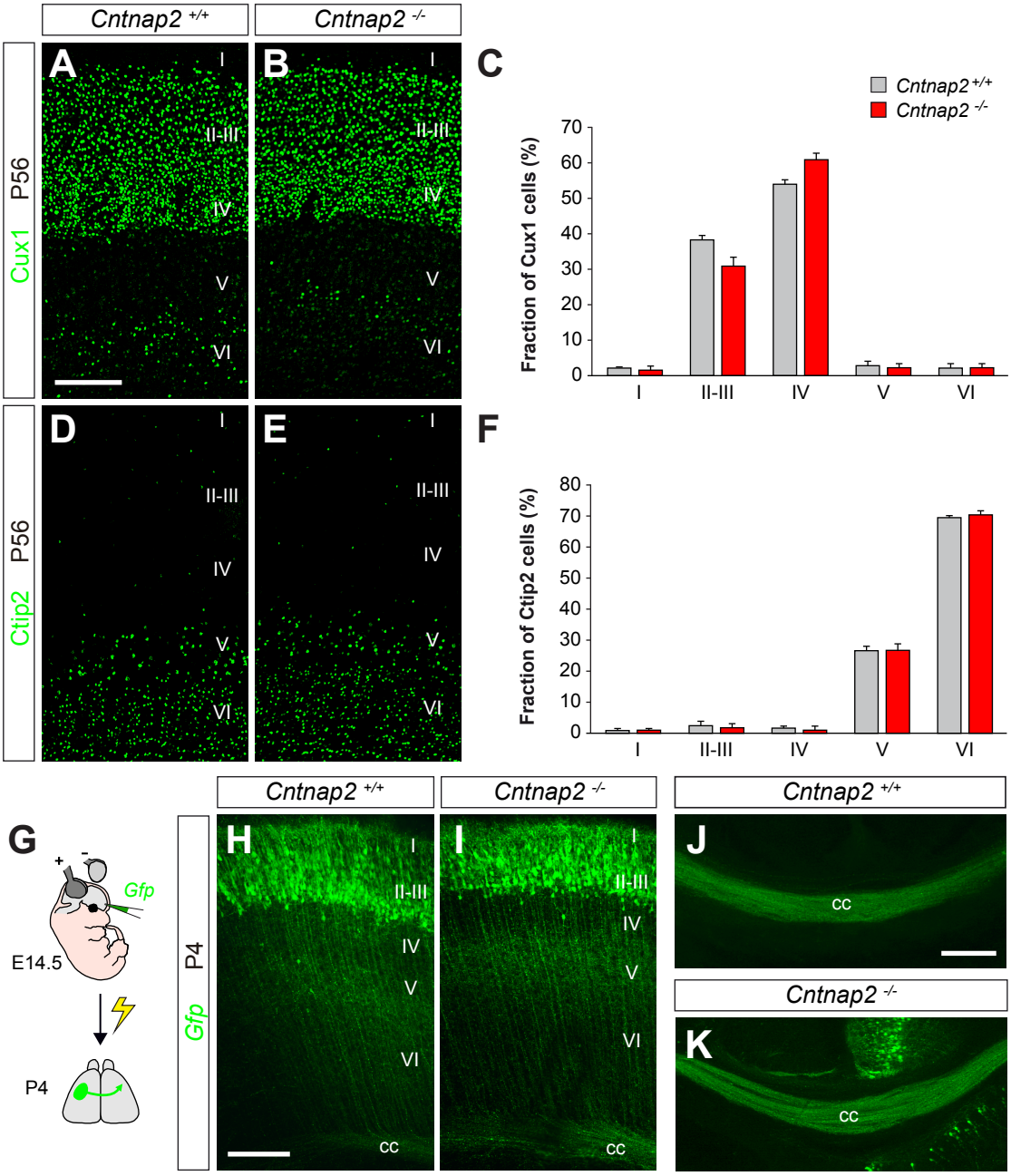

Supplementary Figure 2. Normal distribution of pyramidal cells in the neocortex of adult *Cntnap2* mutant mice. (**A, B, D, E**) Distribution of Cux1+ (A, B) and Ctip2+ (D, E) cells in the somatosensory cortex of 8 weeks old control (A, D) and Cntnap2 mutant (B, E) mice. (**C, F**) Laminar distribution of Cux1+ (C) and Ctip2+ (F) cells in the somatosensory cortex; $n = 4$ control and *Cntnap2* mutant mice; X2 test, $p = 0.573$ (C) and $p = 0.983$ (F). Histograms show average ± SEM. (**G**) Schematic of the experimental design. (**H, I**) Distribution of pyramidal cells born at E14.5 in the somatosensory cortex of control (H) and *Cntnap2* mutant (I) mice. (**J, K**) Axons from layer 2/3 pyramidal cells crossing through the corpus callosum (cc) in control (J) and *Cntnap2* mutant (K) mice. Scale bars equal 200 µm.

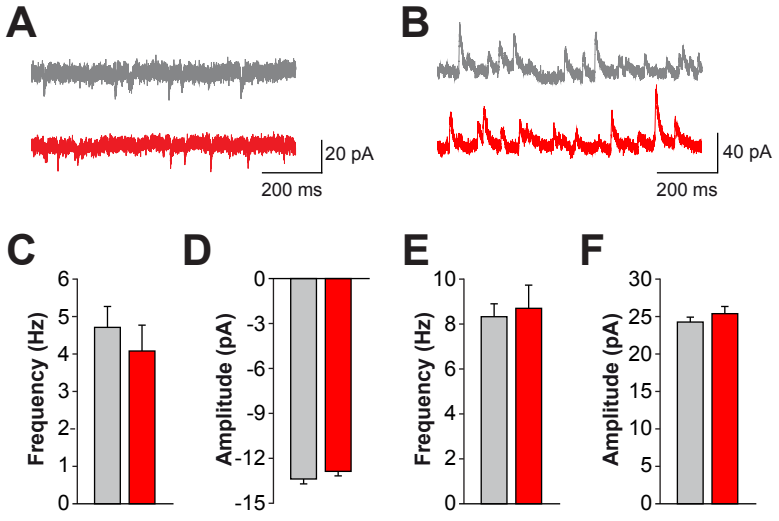

Supplementary Figure 3. Normal organization of excitatory and inhibitory circuits in the neocortex of adult *Cntnap2* mutant mice. (**A, B**) Representative traces of mEPSCs (A) and mIPSCs (B) recordings from layer 2/3 pyramidal cell neurons in the somatosensory cortex of 8 weeks old control and *Cntnap2* mutant mice. (**C, D**) Quantification of mEPSCs frequencies (C) and amplitudes (D) in pyramidal cells; $n = 14$ cells in control and *Cntnap2* mutant mice, respectively; *t*-test, $p = 0.479$ (C) and $p = 0.274$ (D). (**E, F**) Quantification of mIPSCs frequencies (E) and amplitudes (F) in pyramidal cells; $n = 14$ cells in control and *Cntnap2* mutant mice, respectively; *t*-test, $p = 0.289$ (E) and $p = 0.775$ (F). Histograms show average ± SEM.

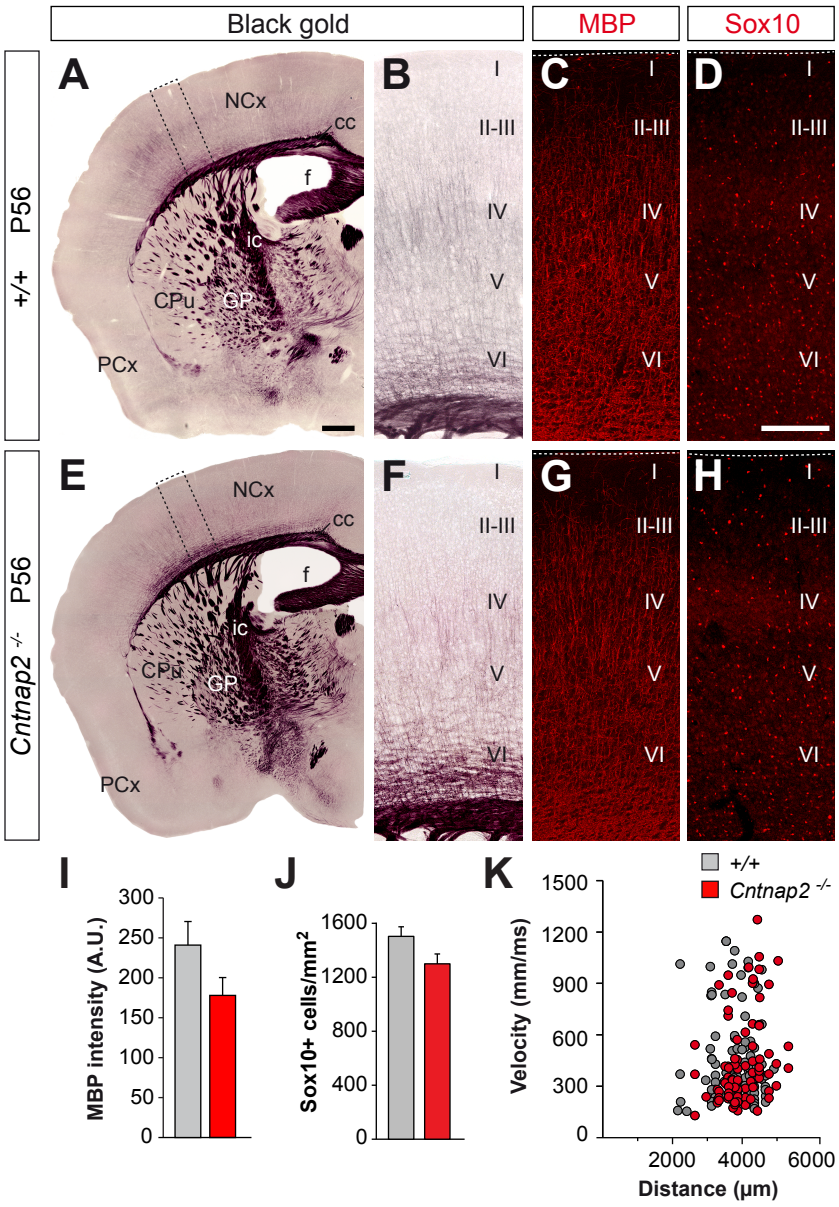

Supplementary Figure 4. Normal myelination in adult *Cntnap2* mutant mice. (**A–D, E–H**) Histological staining of myelin by Black gold (A, B, E, F) and immunohistochemistry for MBP (C, G) and Sox10 (D, H) in the neocortex of 8 weeks old control (A–D) and *Cntnap2* mutant (E–H) mice. (**I**) Quantification of MBP intensity in the somatosensory cortex; $n = 4$ control and 4 *Cntnap2* mutant mice; *t*-test, p = 0.14. (**J**) Quantification of the density of Sox10+ cells in the somatosensory cortex; $n = 4$ control and 4 *Cntnap2* mutant mice, *t*-test, $p = 0.050$. (**K**) Distribution of axonal conductance speeds for individual axons at different distances from the stimulation electrode. Histograms show average ± SEM. Scale bar equals 200 µm.

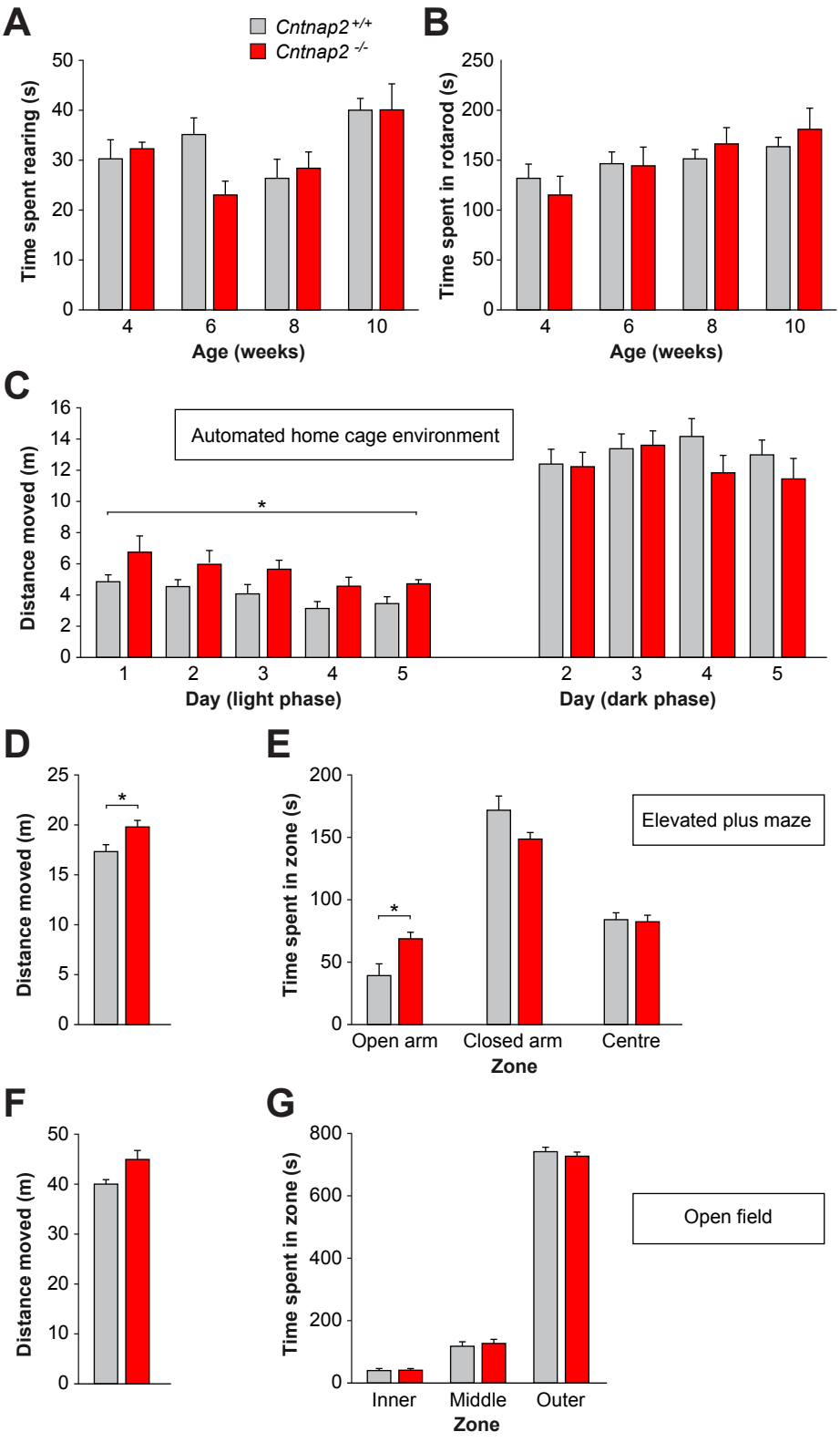

Supplementary Figure 5. Sensorimotor coordination, locomotor performance and anxiety-like behaviors in *Cntnap2* mutant mice. (**A**) Quantification of time spent rearing. (**B**) Quantification of performance in an accelerating rotarod. (**C**) Baseline locomotor activity in light and dark phase during 5 days. (**D**) Distance moved in the elevated plus maze. (**E**) Time spent in each arm of the elevated plus maze. (**F**) Distance moved in 5 minutes in the open field. (**G**) Time spent in each area of the open field in five minutes. Histograms show average ± SEM. n = 11-14 control and 10-12 *Cntnap2* mutant mice; RM-ANOVA (A–C, E, G); one-way ANOVA (D, F); *$p < 0.05$.

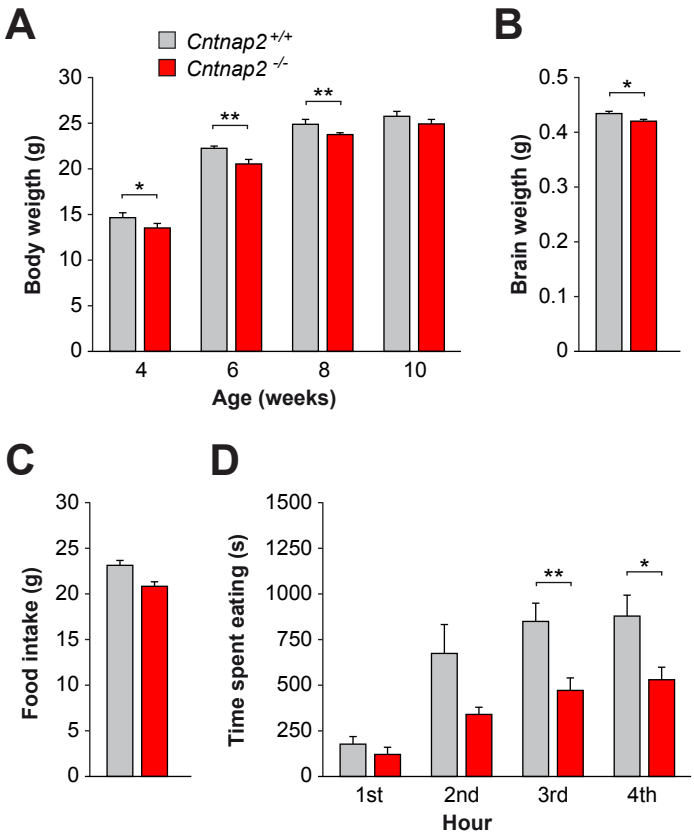

Supplementary Figure 6. Physical measurements in *Cntnap2* mutant mice. (**A**) Quantification of bodyweight during development. (**B**) Quantification of brain weight in adult mice. (**C**) Quantification of total amount of food eaten in 5 days in an automated home cage environment. (**D**) Quantification of time spent eating in a novel environment in the home cage. Histograms show average ± SEM. n = 8-14 control and 8-12 *Cntnap2* mutant mice; RM-ANOVA (A, D); one-way ANOVA (B, C); $^{**}p < 0.01$, $^{*}p < 0.05$.

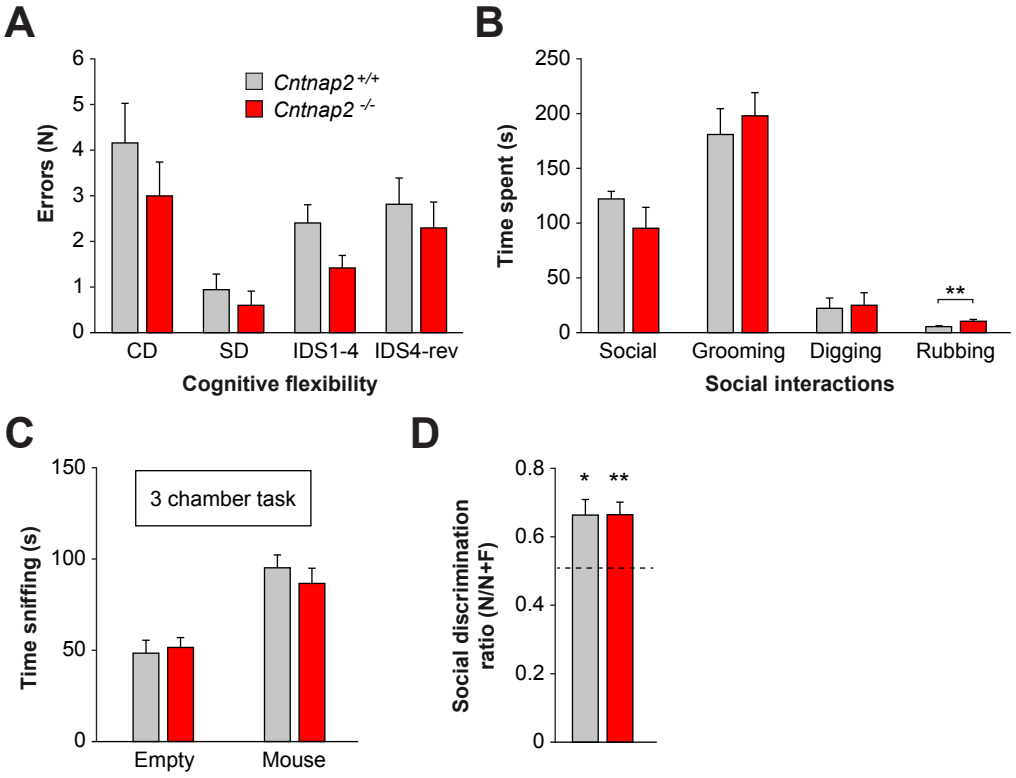

Supplementary Figure 7. Normal social, non-social cognitive and affective tasks in *Cntnap2* mutant mice. (**A**) Quantification of errors needed to reach criterion in the set-shifting task. (**B**) Quantification of time spent on different behaviors during the juvenile social interaction task. (**C**) Quantification of time spent sniffing the mouse or wired cage in the three-chamber paradigm during the sociability phase. (**D**) Discrimination ratio in the three-chamber paradigm during the preference phase. Histograms show average ± SEM. *n* =8-14 control and 8-12 *Cntnap2* mutant mice; RM-ANOVA; **p* < 0.05, ***p* < 0.01.

Supplementary Table 1. Summary of data and statistical analyses.

FIGURE 1	Measurement	Values	N	Statistical	P value
Fig 1L	Kv1.2 clusters per node	Controls, 10 (0), 115 (1), 138 (2)	Controls, *n* = 263 from 3 mice; *Cntnap2* mutants, *n* = 201 from 3 mice	X2 test	p < 0.001 (***)
		Cntnap2 mutants, 32 (0), 114 (1), 55 (2)			
FIGURE 2	Measurement	Values	N	Statistical	P value
Fig 2C	Fiber volley amplitude (mean ± sem)	Controls, -0.24 ± 0.08 mV; *Cntnap2* mutants, -0.07 ± 0.02 mV	Controls, *n* = 8 slices from 5 mice; *Cntnap2* mutants, *n* = 10 slices from 4 mice	Student *t*-test	p < 0.05 (*)
Fig 2E	Anti-peak amplitude (mean ± sem)	Controls, -0.16 ± 0.02 mV; *Cntnap2* mutants, -0.11 ± 0.01 mV	Controls, *n* = 39 axons from 6 mice; *Cntnap2* mutants, *n* = 39 axons from 6 mice	Student *t*-test	p < 0.05 (*)
Fig 2G	Anti-peak amplitude (mean ± sem)	Controls, -0.16 ± 0.02 mV; *Cntnap2* mutants, -0.11 ± 0.01 mV	Controls, *n* = 39 axons from 6 mice; *Cntnap2* mutants, *n* = 39 axons from 6 mice	Student *t*-test	p < 0.05 (*)
FIGURE 3	Measurement	Values	N	Statistical	P value
Fig 3C	Frequency sEPSC (mean ± sem)	Controls, 4.4 ± 0.8 Hz; *Cntnap2* mutants, 4.3 ± 0.5 Hz	Controls, *n* = 13 cells; *Cntanp2* mutants, *n* = 18 cells	Student *t*-test	p = 0.872
Fig 3D	Amplitude sEPSC (mean ± sem)	Controls, -15.3 ± 0.5 pA; *Cntnap2* mutants, -18.5 ± 0.5 pA			p < 0.001 (***)
Fig 3E	Frequency sIPSC (mean ± sem)	Controls, 8.1 ± 0.8 Hz; *Cntnap2* mutants, 8.5 ± 0.7 Hz	Controls, *n* = 13 cells; *Cntanp2* mutants, *n* = 18 cells	Student *t*-test	p = 0.751
Fig 3F	Amplitude sIPSC (mean ± sem)	Controls, 41.7 ± 5.6 pA; *Cntnap2* mutants, 36.3 ± 3.1 pA			p = 0.368
Fig 3L	Amplitude eEPSC (mean ± sem)	Controls, -28.4 ± 3.1 pA; *Cntnap2* mutants, -50.8 ± 4.7 pA	Controls, *n* = 17 cells; *Cntanp2* mutants, *n* = 18 cells	Student *t*-test	p < 0.001 (***)
Fig 3J	Pair-pulse ratio (mean ± sem)	Controls, 1.27 ± 0.15; *Cntnap2* mutants, 0.85 ± 0.07	Controls, *n* = 17 cells; *Cntanp2* mutants, *n* = 18 cells	Student *t*-test	p < 0.05 (*)
Fig 3K	Pair-pulse ratio (mean ± sem)	Controls, 2.08 ± 0.26; *Cntnap2* mutants, 2.03 ± 0.18	Controls, *n* = 14 cells; *Cntanp2* mutants, *n* = 13 cells	Student *t*-test	p = 0.871
FIGURE 4	Measurement	Values	N	Statistical	P value
Fig 4C	Density of PV+ interneurons (mean ± sem)	Layer I: Controls, 2.7 ± 0.5 cells/mm2; *Cntnap2* mutants, 1.3 ± 0.7 cells/mm2	Controls, *n* = 4 mice; *Cntnap2* mutants, *n* = 4 mice	Two way-ANOVA	p = 0.98
		Layer II-III: Controls, 92 ± 6.1 cells/mm2; Cntnap2 mutants, 76 ± 9.9 cells/mm2			
		Layer IV: Controls, 285 ± 16 cells/mm2; *Cntnap2* mutants, 278 ± 13 cells/mm2			
		Layer V: Controls, 251 ± 9 cells/mm2; *Cntnap2* mutants, 239 ± 25 cells/mm2			
		Layer VI: Controls, 109 ± 5.6 cells/mm2; *Cntnap2* mutants, 100 ± 9.6 cells/mm2			
Fig 4F	Density of SST+ interneurons (mean ± sem)	Layer I: Controls, 11 ± 1.1 cells/mm2; *Cntnap2* mutants, 15 ± 4.2 cells/mm2	Controls, *n* = 4 mice; *Cntnap2* mutants, *n* = 4 mice	Two way-ANOVA	p = 0.88
		Layer II-III: Controls, 57 ± 4.3 cells/mm2; *Cntnap2* mutants, 57 ± 9.8 cells/mm2			
		Layer IV: Controls, 86 ± 6.2 cells/mm2; *Cntnap2* mutants, 101 ± 30 cells/mm2			
		Layer V: Controls, 165 ± 17 cells/mm2; *Cntnap2* mutants, 180 ± 20 cells/mm2			
		Layer VI: Controls, 116 ± 8.4 cells/mm2; *Cntnap2* mutants, 124 ± 11 cells/mm2			
Fig 4I	Density of CR+ interneurons (mean ± sem)	Layer I: Controls, 20 ± 2.4 cells/mm2; *Cntnap2* mutants, 23 ± 3.6 cells/mm2	Controls, *n* = 4 mice; *Cntnap2* mutants, *n* = 4 mice	Two way-ANOVA	p = 0.78
		Layer II-III: Controls, 116 ± 6.5 cells/mm2; Cntnap2 mutants, 116 ± 17 cells/mm2			
		Layer IV: Controls, 71 ± 4.8 cells/mm2; *Cntnap2* mutants, 72 ± 9.4 cells/mm2			
		Layer V: Controls, 52 ± 7.8 cells/mm2; *Cntnap2* mutants, 70 ± 20 cells/mm2			
		Layer VI: Controls, 22 ± 3.3 cells/mm2; *Cntnap2* mutants, 30 ± 12 cells/mm2			
FIGURE 5	Measurement	Values	N	Statistical	P value
Fig 5E	Intensity MBP (mean ± sem)	Controls, 200 ± 7.6 (A.U.); *Cntnap2* mutants, 151 ± 12 (A.U.)	Controls, *n* = 3; *Cntnap2* mutants, *n* = 3	Student *t*-test	p < 0.001 (***)
Fig 5J	Density of Sox10+ cells (mean ± sem)	Controls, 1363 ± 77 cells/mm2; *Cntnap2* mutants, 910 ± 27 cells/mm2	Controls, *n* = 4; *Cntnap2* mutants, *n* = 4	Student *t*-test	p < 0.01 (**)
Fig 5L	Instantaneous velocity (mean ± sem)	0-1000 µm: Controls, 185.3 ± 16.51 µm/ms; *Cntnap2* mutants, 176.53 ± 4.15 µm/ms	Controls, *n* = 152 from 5 mice; *Cntnap2* mutants, *n* = 187 from 7 mice	Two way-ANOVA	p = 0.85
		1000-2000 µm: Controls, 262.95 ± 19.70 µm/ms; *Cntnap2* mutants, 259.56 ± 14.79 µm/ms			p = 0.96
		2000-3000 µm: Controls, 309.65 ± 16.27 µm/ms; *Cntnap2* mutants, 300.71 ± 24.23 µm/ms			p = 0.79
		3000-4000 µm: Controls, 518.20 ± 92.71 µm/ms; *Cntnap2* mutants, 289.03 ± 17.50 µm/ms			p < 0.001 (***)
		4000-6000 µm: Controls, 467.55 ± 53.23 µm/ms; *Cntnap2* mutants, 316.90 ± 20.12 µm/ms			p < 0.001 (***)
FIGURE 6	Measurement	Values	N	Statistical	P value
Fig 6A	Time spent grooming (mean ± sem)	4 weeks: Controls, 21,665 ± 2,503 s; *Cntnap2* mutants, 32,558 ± 7,184 s	Controls, *n* = 11 mice; *Cntnap2* mutants, *n* = 10 mice	RM-ANOVA	p = 0.153
		6 weeks: Controls, 7.604 ± 2.367 s; *Cntnap2* mutants, 60.073 ± 8.546 s			p < 0.001 (***)
		8 weeks: Controls, 16.375 ± 3.210 s; *Cntnap2* mutants, 39.215 ± 5.444 s			p < 0.001 (***)
		10 weeks: Controls, 8.702 ± 2.634 s; *Cntnap2* mutants, 35.632 ± 7.776 s			p < 0.01 (**)
Fig 6B	Time spent ear rubbing (mean ± sem)	4 weeks: Controls, 0.305 ± 0.264 s; *Cntnap2* mutants, 1.672 ± 0.973 s	Controls, *n* = 11 mice; *Cntnap2* mutants, *n* = 10 mice	RM-ANOVA	p = 0.173
		6 weeks: Controls, 0.000 ± 0.000 s; *Cntnap2* mutants, 20.085 ± 3.960 s			p < 0.001 (***)
		8 weeks: Controls, 0.000 ± 0.000 s; *Cntnap2* mutants, 15.224 ± 3.039 s			p < 0.001 (***)
		10 weeks: Controls, 0.000 ± 0.000 s; *Cntnap2* mutants, 8.345 ± 3.070 s			p < 0.05 (*)
Fig 6C	Number of involuntary movements (mean ± sem)	4 weeks: Controls, 0.455 ± 0.207; *Cntnap2* mutants, 1.300 ± 0.496	Controls, *n* = 11 mice; *Cntnap2* mutants, *n* = 10 mice	RM-ANOVA	p = 0.070
		6 weeks: Controls, 0.455 ± 0.207; *Cntnap2* mutants, 3.300 ± 1.155			p < 0.001 (***)
		8 weeks: Controls, 0.364 ± 0.203; *Cntnap2* mutants, 3.200 ± 0.680			p < 0.001 (***)
		10 weeks: Controls, 0.091 ± 0.091; *Cntnap2* mutants, 2.800 ± 0.892			p < 0.001 (***)

Fig 6D	Distance moved (mean ± sem)	Light phase: Controls, 418.095 ± 26,817 cm; *Cntnap2* mutants, 569.950 ± 66.534 cm	Controls, *n* = 14 mice; *Cntnap2* mutants, *n* = 12 mice	RM-ANOVA	p < 0.05 (*)
		Dark phase: Controls, 1327.259 ± 85.854 cm; *Cntnap2* mutants, 1213.761 ± 93.006 cm			p = 0.379
Fig 6E	Distance moved (mean ± sem)	Controls, 8098.950 ± 341.567 cm; *Cntnap2* mutants, 9761.231 ± 447.054 cm	Controls, *n* = 14 mice; *Cntnap2* mutants, *n* = 12 mice	One way-ANOVA	p < 0.01 (**)
FIGURE S2	Measurement	Values	N	Statistical	P value
Fig S2C	Fraction of Cux1+ interneurons (mean ± sem)	Layer I: Controls, 2.08 ± 0.23 %; *Cntnap2* mutants, 1.58 ± 0.23%	Controls, *n* = 4 mice; *Cntnap2* mutants, *n* = 4 mice	X2 test	p = 0.573
		Layer II-III: Controls, 38.98 ± 0.76%; *Cntnap2* mutants, 32.00 ± 1.22 %			
		Layer IV: Controls, 54.41 ± 0.76%; *Cntnap2* mutants, 61.52 ± 1.35 %			
		Layer V: Controls, 2.54 ± 0.30 %; *Cntnap2* mutants, 2.37 ± 0.30%			
		Layer VI: Controls, 1.98 ± 0.34 %; *Cntnap2* mutants, 2.53 ± 0.40 %			
Fig S2F	Fraction of Ctip2+ interneurons (mean ± sem)	Layer I: Controls, 1.04 ± 0.07 %; *Cntnap2* mutants, 0.69 ± 0.06 %	Controls, *n* = 4 mice; *Cntnap2* mutants, *n* = 4 mice	X2 test	p = 0.983
		Layer II-III: Controls, 2.43 ± 0.13 %; Cntnap2 mutants, 1.55 ± 0.11 %			
		Layer IV: Controls, 1.66 ± 0.10 %; *Cntnap2* mutants, 1.21 ± 0.08 %			
		Layer V: Controls , 25.99 ± 0.93 %; *Cntnap2* mutants, 26.77 ± 0.88 %			
		Layer VI: Controls, 68.87 ± 1.02 %; *Cntnap2* mutants, 69.77 ± 0.92 %			
FIGURE S3	Measurement	Values	N	Statistical	P value
Fig S3C	Frequency mEPSC (mean ± sem)	Controls, 4.7 ± 0.5 Hz; *Cntnap2* mutants, 4.1 ± 0.6 Hz	Controls, *n* = 14 cells; *Cntanp2* mutants, *n* = 14 cells	Student *t*-test	p = 0.479
Fig S3D	Amplitude mEPSC (mean ± sem)	Controls, -13.3 ± 0.3 pA; *Cntnap2* mutants, -12.7 ± 0.5 pA			p = 0.274
Fig S3E	Frequency mIPSC (mean ± sem)	Controls, 8.3 ± 0.6 Hz; *Cntnap2* mutants, 8.6 ± 1.1 Hz	Controls, *n* = 14 cells; *Cntanp2* mutants, *n* = 14 cells	Student *t*-test	p = 0.289
Fig S3F	Amplitude mIPSC (mean ± sem)	Controls, 23.7 ± 0.7 pA; *Cntnap2* mutants, 25.0 ± 0.7 pA			p = 0.775
FIGURE S4	Measurement	Values	N	Statistical	P value
Fig S4G	Intensity MBP (mean ± sem)	Controls, 238 ± 29 (A.U.); *Cntnap2* mutants, 178 ± 17 (A.U.)	Controls, *n* = 4; *Cntnap2* mutants, *n* = 4	Student *t*-test	p = 0.136
Fig S4J	Density of Sox10+ cells (mean ± sem)	Controls, 1489 ± 70 cells/mm2; *Cntnap2* mutants, 1287 ± 72 cells/mm2	Controls, *n* = 4; *Cntnap2* mutants, *n* = 4	Student *t*-test	p = 0.050
FIGURE S5	Measurement	Values	N	Statistical	P value
Fig S5A	Time spent rearing behaviour (mean ± sem)	4 weeks: Controls, 29.953 ± 3.935 s; *Cntnap2* mutants, 31.708 ± 1.963 s	Controls, *n* = 11 mice; *Cntnap2* mutants, *n* = 10 mice	RM-ANOVA	p = 0.111
		6 weeks: Controls, 35.077 ± 3.384 s; *Cntnap2* mutants, 22.592 ± 3.234 s			p = 0.934
		8 weeks: Controls, 26.647 ± 3.450 s; *Cntnap2* mutants, 28.168 ± 3.381 s			p = 0.893
		10 weeks: Controls, 39.565 ± 2.879 s; *Cntnap2* mutants, 40.040 ± 5.177 s			p = 0.218
Fig S5B	Time spent in rotarod (mean ± sem)	4 weeks: Controls, 132.143 ± 13.692 s; *Cntnap2* mutants, 113.250 ± 17.969 s	Controls, *n* = 14 mice; *Cntnap2* mutants, *n* = 12 mice	RM-ANOVA	p = 0.301
		6 weeks: Controls, 148.714 ± 9.846 s; *Cntnap2* mutants, 145.000 ± 18.841 s			p = 0.060
		8 weeks: Controls, 151.500 ± 9.735 s; *Cntnap2* mutants, 167.250 ± 15.416 s			p = 0.069
		10 weeks: Controls, 163.429 ± 9.181 s; *Cntnap2* mutants, 182.583 ± 15.887 s			p = 0.271
Fig S5C	Distance moved, Light phase (mean ± sem)	Day 1: Controls, 488.432 ± 38,467 cm; *Cntnap2* mutants, 676.232 ± 98.868 cm	Controls, *n* = 14 mice; *Cntnap2* mutants, *n* = 12 mice	RM-ANOVA	p < 0.05 (*)
		Day 2: Controls, 451.954 ± 34.605 cm; *Cntnap2* mutants, 592.582 ± 79.757 cm			
		Day 3: Controls, 410.479 ± 47.578 cm; *Cntnap2* mutants, 558.989 ± 78.343 cm			
		Day 4: Controls, 321.516 ± 20.207 cm; *Cntnap2* mutants, 451.999 ± 52.317 cm			
		Day 5: Controls, 344.033 ± 51.782 cm; Cntnap2 mutants, 468.766 ± 40.395 cm			
	Distance moved, Dark phase (mean ± sem)	Day 2: 1249.904 ± 83.625 cm; *Cntnap2* mutants, 1249.904 ± 83.625 cm			p = 0.438
		Day 3: Controls, 1343.068 ± 82.003 cm; *Cntnap2* mutants, 1339.427 ± 108.971 cm			
		Day 4: Controls, 1418.947 ± 104.268 cm; *Cntnap2* mutants, 1174.986 ± 110.317 cm			
		Day 5: Controls, 1280.005 ± 105.911 cm; *Cntnap2* mutants, 1137.073 ± 142.558 cm			
Fig S5D	Distance moved (mean ± sem)	Controls, 1720.811 ± 72.897 cm; *Cntnap2* mutants, 1954.860 ± 94.937 cm	Controls, *n* = 14 mice; *Cntnap2* mutants, *n* = 12 mice	One way-ANOVA	p < 0.05 (*)
Fig S5E	Time spent in zone (mean ± sem)	Open arm: Controls, 41.000 ± 7.878 s; *Cntnap2* mutants, 69.130 ± 6.781 s	Controls, *n* = 14 mice; *Cntnap2* mutants, *n* = 12 mice	RM-ANOVA	p < 0.05 (*)
		Close arm: Controls, 174.249 ± 9.390 s; *Cntnap2* mutants, 148.160 ± 6.172 s			p = 0.112
		Centre: Controls, 83.749 ± 6.360 s; *Cntnap2* mutants, 81.553 ± 5.263 s			p = 0.384
Fig S5F	Distance moved (mean ± sem)	Controls, 4062.214 ± 118.702 cm; *Cntnap2* mutants, 4564.070 ± 228.164 cm	Controls, *n* = 14 mice; *Cntnap2* mutants, *n* = 12 mice	One way-ANOVA	p = 0.053
Fig S5G	Time spent in zone (mean ± sem)	Inner: Controls, 10.691 ± 1.335 s; *Cntnap2* mutants, 9.023 ± 1.093 s	Controls, *n* = 14 mice; *Cntnap2* mutants, *n* = 12 mice	RM-ANOVA	p = 0.353
		Middle: Controls, 33.823 ± 2.504 s; *Cntnap2* mutants, 33.497 ± 2.759 s			p = 0.931
		Outer: Controls, 255.486 ± 3.343 s; *Cntnap2* mutants, 257.480 ± 3.599 s			p = 0.688
FIGURE S6	Measurement	Values	N	Statistical	P value
Fig S6A	Body weigth (mean ± sem)	4 weeks: Controls, 14.571 ± 0.451 g; *Cntnap2* mutants, 13.296 ± 0.390 g	Controls, *n* = 14 mice; *Cntnap2* mutants, *n* = 12 mice	RM-ANOVA	p < 0.05 (*)
		6 weeks: Controls, 22.106 ± 0.265 g; *Cntnap2* mutants, 20.567 ± 0.442 g			p < 0.01 (**)
		8 weeks: Controls, 24.927 ± 0.213 g; *Cntnap2* mutants, 23.471 ± 0.327 g			p < 0.01 (**)
		10 weeks: Controls, 25.930 ± 0.417 g; *Cntnap2* mutants, 24.789 ± 0.381 g			p = 0.058

Fig S6B	Brain weigth (mean ± sem)	Controls, 0.436 ± 0.005 g; *Cntnap2* mutants, 0.419 ± 0.006 g	Controls, *n* = 8 mice; *Cntnap2* mutants, *n* = 8 mice	One way-ANOVA	p < 0.05 (*)
Fig S6C	Food intake (mean ± sem)	Controls, 23.303 ± 1.141 g; *Cntnap2* mutants, 21.000 ± 0.746 g	Controls, *n* = 14 mice; *Cntnap2* mutants, *n* = 12 mice	One way-ANOVA	p = 0.117
Fig S6D	Time spent eating (mean ± sem)	1st h: Controls, 182.388 ± 33.782 s; *Cntnap2* mutants, 130.262 ± 37.671 s	Controls, *n* = 13 mice; *Cntnap2* mutants, *n* = 11 mice	RM-ANOVA	p = 0.313
		2nd h: Controls, 677.538 ± 166.370 s; *Cntnap2* mutants, 336.465 ± 41.818 s			p = 0.079
		3rd h: Controls, 861.305 ± 108.653 s; *Cntnap2* mutants, 485.069 ± 62.639 s			p < 0.01 (**)
		4th h: Controls, 894.006 ± 124.339 s; *Cntnap2* mutants, 527.927 ± 82.261 s			p < 0.05 (*)
FIGURE S7	Measurement	Values	N	Statistical	P value
Fig S7	Number of errors (mean ± sem)	CD: Controls, 4.143 ± 0.889; *Cntnap2* mutants, 3.000 ± 0.769	Controls, *n* = 14 mice; *Cntnap2* mutants, *n* = 12 mice	RM-ANOVA	p = 0.158
		SD: Controls, 0.929 ± 0.355; *Cntnap2* mutants, 0.583 ± 0.313			p = 0.432
		IDS1-4: Controls, 2.393 ± 0.403; *Cntnap2* mutants, 1.417 ± 0.277			p = 0.051
		IDS4-rev: Controls, 2.786 ± 0.595; *Cntnap2* mutants, 2.250 ± 0.605			p = 0.719
Fig S7B	Time spent (mean ± sem)	Social Controls, 121.720 ± 7.959 s; *Cntnap2* mutants, 96.945 ± 18.246 s	Controls, *n* = 10 mice; *Cntnap2* mutants, *n* = 8 mice	RM-ANOVA	p = 0.127
		Grooming: Controls, 183.624 ± 22.327 s; *Cntnap2* mutants, 199.110 ± 21.323 s			p = 0.051
		Digging: Controls, 24.256 ± 7.414 s; *Cntnap2* mutants, 26.680 ± 12.387 s			p = 0.863
		Rubbing: Controls, 7.224 ± 2.148 s; *Cntnap2* mutants, 12.920 ± 2.397 s			p < 0.01 (**)
Fig S7C	Time sniffing (mean ± sem)	Empty: Controls, 47.805 ± 6.592 s; *Cntnap2* mutants, 51.040 ± 6.357 s	Controls, *n* = 8 mice; *Cntnap2* mutants, *n* = 10 mice	RM-ANOVA	p = 0.731
		Mouse: Controls, 93.465 ± 9.044 s; *Cntnap2* mutants, 85.752 ± 8.079 s			p = 0.534
Fig S7D	Social discrimination ratio (mean ± sem)	Controls, 0.654 ± 0.037	Controls, *n* = 8 mice; *Cntnap2* mutants, *n* = 10 mice	Student *t*-test	p < 0.05 (*)
		Cntnap2 mutants, 0.652 ± 0.043			p < 0.01 (**)

Supplementary Table 2. Developmental Shirpa screening in control and *Cntnap2* mutant mice.

		Controls	Mutants	Controls	Mutants	Controls	Mutants	Controls	Mutants
	Age (weeks)	4		6		8		10	
Body Position	Active	14	12	14	12	14	12	14	12
Tremor	Absent	14	12	14	12	14	12	14	12
Palpebral closure	Eyes open	14	12	14	12	14	12	14	12
Coat appearance	Tidy & groomed	14	12	14	12	14	12	14	12
Whiskers	Present	14	12	14	12	14	12	14	12
Lacrimation	Eyes clean	14	12	14	12	14	12	14	12
Defecation	Quantity	2,14	1,58	2	2,83	3,36	3,92	1,86	1,75
Transfer arousal	Immediate movement	14	12	14	12	14	12	14	12
Gait	Fluid	14	12	14	12	14	12	14	12
Tail elevation	Horizontal	14	11	10	9	7	9	8	7
Startle response	Preyer reflex	14	12	14	12	14	12	14	12
Touch escape	No response	0	2	1	2	1	0	5	6
	Response to touch	14	7	12	8	10	9	9	6
	Flees prior to touch	0	3	1	2	3	3	0	0
Positional passivity	Struggles	14	12	14	11	14	12	14	12
Trunk curl	Absent	14	12	14	11	14	12	14	12
Limb grasping	Absent	14	12	14	11	14	12	14	12
Skin color	Pink	14	12	14	11	14	12	14	12
Pinna reflex	Present	14	12	14	11	14	12	14	12
Corneal reflex	Present	14	12	14	11	14	12	14	12
Evidence of biting	None	9	11	14	11	14	12	14	12
Squeaks	Present	14	4	12	5	9	3	10	3
Grip	OK	14	12	14	11	14	12	14	12
Puberty	In Development	10	9	4	5	0	1	0	0
	Full puberty	1	1	9	5	14	11	14	12

Extended Material and Methods

Animals

The local ethical committees at the Instituto de Neurociencias, University Medical Center Utrecht, and King's College London approved all experimental procedures involving animals. For behavioral experiments, homozygous Cntnap2 mutant males (Poliak S et al. 2003) were directly obtained from Jackson (Bar Harbor, Maine, USA) and used for breeding with C57BL/6J females. First generation heterozygous offspring were used for breeding pairs in order to generate littermate control and Cntnap2 mutant mice for behavioral experiments.

Histology

The following secondary antibodies (all from Molecular Probes) were used for immunohistochemistry: donkey anti-mouse 647 (1:200, A-31571), donkey anti-rat 488 (1:200, A21208), donkey anti-rabbit 555 (1:200, A31572), donkey anti-rat 488 (1:200, A21208), donkey anti-mouse 647 (1:200, A21240), donkey anti-rabbit 488 (1:200, A21206), goat anti mouse IgG2b 555 (1:200, A21147), donkey anti-mouse 488 (1:200, A21202), and goat anti-guinea pig 546 (1:200, A11074). Cell nuclei were stained with 4"-6-diamidino-2-phenylindole (DAPI) in PBS and sections mounted with Mowiol (Sigma). For Black gold stainings, 40 μm free-floating sections were processed following the manufacturer's protocol (Black gold II Myelin Staining Kit, AG105, Merk Millipore).

In utero electroporation

E14.5 timed-pregnant mice were deeply anesthetized and the abdominal cavity cut open. Embryos were exposed in the uterus, and *pCAG-Gfp* plasmid (1 μg/μl) was injected into the lateral ventricle of the telencephalon through the uterine wall. Square electric pulses of

45 V and 50 ms were passed through the uterus five times, spaced 950 ms, using a square pulse electroporator. The uterine horns were placed back in the abdominal cavity, which was then suture closed and the female was allowed to recover.

Electrophysiology

Juvenile animals were anesthetized with pentobarbital and transcardially perfused with cold 95% O_2 + 5% CO_2 sucrose artificial cerebrospinal fluid (aCSF) containing (in mM): 70 sucrose, 86 NaCl, 4 KCl, 1 NaH_2PO_4, 0.5 $CaCl_2$, 7 $MgSO_4$, 26 $NaHCO_3$, 25 glucose, pH 7.3-7.4, 300-315 mOsm. Animals were then decapitated and the brain was placed in cold sucrose aCSF. Coronal slices (350 μm) were cut using a Leica vibratome (Leica VT 1200S). Then, they were stored at room temperature for at least 1 hour in a submerged holding chamber with 95% O_2/5% CO_2 recording aCSF. For adult animals, we prepared slices (300 μm) as described before (Ting JT et al. 2014) with small modifications. Cold 95% O_2 + 5% CO_2 NMDG-HEPES solution was used for perfusion and slicing instead of sucrose aCSF. This solution contained (in mM): 93 NMDG, 2.5 KCl, 1.25 NaH_2PO_4, 0.5 $CaCl_2$, 10 $MgSO_4$, 30 $NaHCO_3$, 25 glucose, 20 HEPES, 2 thiourea, 3 sodium pyruvate, 5 sodium ascorbate, pH 7.3-7.4, 300-315 mOsm. Adolescent and adult slices had an initial protective recovery period of 12-15 min at 32ºC in NMDG-HEPES aCSF. Then, they were stored at room temperature for at least 1 hour in a submerged holding chamber with 95% O_2/5% CO_2 NaCl-HEPES solution containing (in mM): 92 NaCl, 2.5 KCl, 1.25 NaH_2PO_4, 2 $CaCl_2$, 2 $MgSO_4$, 30 $NaHCO_3$, 25 glucose, 20 HEPES, 2 thiourea, 3 sodium pyruvate, 5 sodium ascorbate pH 7.3-7.4, 300-315 mOsm. Each slice was transferred to a submerged recording chamber and continuously perfused (2.5-3 ml/min) with recording aCSF solution through a peristaltic pump (Gilson). The composition of the recording aCSF was (in mM):

125 NaCl, 2.5 KCl, 1.25 NaH_2PO_4, 2.5 $CaCl_2$, 1.3 $MgCl_2$, 26 $NaHCO_3$, 10 glucose, pH 7.4 when equilibrated with 95% O_2 + 5% CO_2. Recordings were performed at 22-24°C.

For extracellular recordings, stimulation of the corpus callosum was performed with a bipolar stimulating electrode (tungsten wires, 75 μm tip separation, 2 MΩ, WPI), and voltage pulses of 20-30 μs were applied each 30 s by ISO STIM 01D (NPI Electronic). The next antagonists were applied to the recording aCSF to block the synaptic transmission: NBQX (50 μM), picrotoxin (100 μM), AP5 (50 μM) and CGP52432 (5 μM). For fiber volley recordings, stimulation was adjusted to the maximal response across recordings. Identical stimulation was applied among slices from the same region, and recordings were made through patch pipettes filled with extracellular recording solution (1MΩ resistance). For single axon recording, stimulation was adjusted to the minimal all or nothing response. Loose patch recordings of individual axon activity were performed with patch pipettes filled with extracellular recording aCSF (8-10MΩ resistance). Recordings were performed with a Multiclamp 700B amplifier (Molecular Devices), digitized with Digidata 1440A (Molecular Devices) and collected at a sampling frequency of 5 kHz.

Somatic patch-clamp recordings in whole-cell configuration were made from cortical layer 2/3 pyramidal neurons under visual guidance with infrared-differential interference optics (Olympus U-TLUIR) through a 40x water-immersion objective. Patch pipettes were pulled from borosilicate glass capillaries (WPI) with a vertical puller (PC-10, Narishige) and filled with (in mM): 130 CH_3CsSO_3, 4 KCl, 10 HEPES, 4 Na-ATP, 0.4 Na-GTP, 2 $MgCl_2$, and 1 EGTA (pH 7.3, ~290 mΩ). In patch-clamp recordings from juvenile mice, Cs-gluconate was used instead of CH_3CsSO_3. In a subset of neurons, Neurobiotin (2 μg/ml, Vector Labs) or Alexa Fluor 555 (5 mM, Thermo Fisher Scientific) was included to the

intracellular solution for morphological confirmation. Patch pipettes filled with this solution had resistances of 3-5 MΩ. Excitatory currents were recorded at a holding potential of –70 mV (close to the chloride equilibrium potential) and inhibitory currents at +10 mV (reversal potential of glutamatergic events). For the recordings of miniature currents, tetrodotoxin (1 μM, Alomone Laboratories) was applied to the extracellular solution.

For the intracellular recordings of evoked currents in layer 2/3 pyramidal neurons, stimulation of the corpus callosum was performed with a bipolar stimulating electrode (tungsten wires, 75 μm tip separation, 2 MΩ, WPI) positioned under visual control on the callosal tract as described earlier (Kumar SS and JR Huguenard 2001) while the membrane potential was held at –70 mV. Paired pulses (20 Hz) of 30-50 μs were applied at 0.1 Hz by ISO STIM 01D (NPI Electronic). Minimal voltage stimulation to evoke all-or-none postsynaptic responses was determined and then stimuli were applied at slightly above threshold (1.2-1.3 threshold) to reduce the contribution from polysynaptic connections. To exclusively study excitatory responses and to reduce polysynaptic signals, picrotoxin (100 μM) was included in the recording aCSF to block all $GABA_A$-receptor-mediated responses. To avoid the hyperexcitability induced by the blockade of the inhibitory connectivity, the extracellular concentration of divalent ions was increased to 6.5 mM by the application of 4 mM $MgSO_4$. When extracellular calcium was reduced from 2.5 mM to 1 mM, we replaced $CaCl_2$ by $MgSO_4$ equimolar to maintain the divalent concentration. QX-314 bromide (5 μM, Tocris) was included in the intracellular solution to block the generation of action potentials. Patch-clamp recordings were performed in voltage-clamp mode with a Multiclamp 700B amplifier (Molecular Devices), filtered online at 3 kHz, digitized with Digidata 1440A (Molecular Devices) and collected at 20 kHz. Liquid

junction potential (~10 mV) was corrected. Cells with series resistance higher than 25 MΩ were not included. All chemicals and drugs were obtained from Sigma-Aldrich unless otherwise stated. Data analysis was performed off-line with Clampfit 10.2 (Molecular Devices) and Mini Analysis (Synaptosoft). Paired-pulse ratio (PPR) was calculated as the ratio between the amplitude (pA) of the second and first response of the paired stimulus. In fiber volley experiments, slices were considered as biological replicates. For single-axon experiments, axons were considered as biological replicates. Finally, for patch-clamp recordings, neurons represent biological replicates. The events recorded for each biological replicate (about 10-50 fiber volleys, about 10-50 action potentials, about 100-200 spontaneous excitatory/inhibitory postsynaptic currents, about 10-50 evoked excitatory postsynaptic currents) were considered as technical replicates.

Image analysis and quantification

For the quantification of Kv1.2 clustering, images with Kv1.2 and Cntnap1 co-stainings were quantified using customized software written in MATLAB (Mathworks). Nodes were unambiguously identified using Cntnap1 staining, and automatically plots with the mean intensity of Kv1.2 expression were measured across 5 microns adjacent to the identified nodes. The frequency of Kv1.2+ clusters per node was then scored and expressed as frequency of Kv1.2 clusters per node. The animals used represent biological replicates. For each animal, 3-4 fields of view were imaged at the corpus callosum. In each image, about 20 to 30 nodes were selected for quantification.

For the quantification of myelination, overall image directionality and mean intensity were quantified using customized scripts written in MATLAB (Mathworks). Using the Sobel operator (gradient function), MBP maximum and minimum directions and their

respective distribution were determined. Polarity index of each image was computed by taking ratio of the difference in Max and Min directions frequencies over the sum of the max and min frequencies. For quantification of MBP levels, mean intensity from each image was computed after background subtraction. Animals used represent biological replicates. For each animal, about 10-12 sections were imaged and quantified as technical replicates.

Behavior

During development, control and mutant mice were tested once per developmental time point (4, 6 and 8 weeks old). From 10 weeks on (adulthood), mice were additionally exposed to behavioral testing paradigms to assess adult levels of exploratory and anxiety-like behaviors, and set-shifting capacity. A second batch of control and mutant mice were tested for juvenile social interaction at 3 weeks of age and for 3-chamber performance during adulthood. After each trial in each experiment, the test apparatus was cleaned using Trigene solution (0.5 %). Biological replicates are defined as single animals. Repeated measurements or multiple trials of the same animal are considered as technical replicates.

Juvenile social interaction task. P21 mice were placed in a Type 2 Macrolon cage with bedding for 10 minutes and exposed to an unfamiliar, genotype, sex and age matched mouse. The time spent in social interaction as well as other behaviors were manually and blind for genotype scored using Observer software (ObserverXT 10.5, Noldus Information Technology, Wageningen, The Netherlands).

General measures. Both onset of puberty and body weight were measured during development at three different developmental time points (4, 6 and 8 weeks old) and during adulthood (10 weeks old). Onset of puberty was determined by assessing the

progression of balano-preputial separation and scored as 0 (no separation), 1 (separation but not full) or 2 (full separation).

Extended SHIRPA screen. The extended SHIRPA screen was performed as described previously (Molenhuis RT et al. 2014). In short, mice were first placed in a circular jar and visually observed, where, among others, body position, reflexes, coat appearance, and startle response were measured. Next to that, mice were allowed to freely move for 5 minutes in a Type 3 Macrolon cage without bedding. Locomotor activity was measured by video tracking software (Ethovision 9.0, Noldus Information Technology, Wageningen, The Netherlands) and behavior was blindly scored using Observer software (ObserverXT 10.5, Noldus Information Technology). The behavior was defined by scoring the different phases of grooming (Kalueff AV et al. 2016), and explorative rearing behavior.

Rotarod. Each trial consisted of an accelerated speed mode during which the Rotarod (Rotarod 47600, UgoBasile, Varese, Italy) accelerated from 4 to 64 rpm in 5 minutes. Total time that the mice spent on the rotating rod was measured and was ended when mice fell of or 2 consecutive full rotations were observed while the test animal was grasping to the rod.

Open field. Animals were placed in a circular arena of 80 cm diameter and allowed to move freely for 5 minutes. Locomotor activity was measured as distance moved through video tracking software (Ethovision 7.0). In addition, time spent in center, middle and outer zones was analyzed to estimate anxiety levels.

Elevated plus maze. Mice were tested for 5 min and locomotor activity was recorded by video tracking software (Ethovision 7.0). Duration and frequencies of entries into each arm were measured, as well as the total distance moved.

Home cage screening. Mice were housed individually in the automated home environments buildup of clear, Perspex Cages with bedding material and equipped with a PhenoTyper top unit (Noldus Information Technology). The top unit featured a built-in infrared sensitive camera to acquire video tracking of movements independent of lighting conditions. The cages further contained a sheltered house, two feeding stations and a water bottle providing *ad libitum* access to food and water (Kas MJ et al. 2008). Infrared sensors at the feeding platforms and drinking bottle allowed recordings of food and water intake. Food intake was also measured by weighing the food before and after the experiment. Mice were housed in the automated home cage environment for five consecutive days.

Food burying task. Mice were food restricted 24 h prior to testing. At the start of the test, mice were habituated to Macrolon Type 3 cages with fresh double bedding material. Subsequently, mice were placed in a similar new cage (test environment) with 1 piece of chow hidden in the bedding material. The time needed to find the buried piece of chow was considered as a measure for smell perception (Yang M, K Perry, et al. 2011).

Set shifting paradigm. Mice were required to learn the location of a hidden food reward in one of two cups in the test cage. The reward was associated to either a medium (context) or an odor (smell). The task was performed as previously described (Molenhuis RT *et al*. 2014). In short, the latency to find the reward, the number of trials to reach criterion and the number of errors were recorded for each of the seven test phases; simple discrimination, complex discrimination, 4 intradimensional shifts and finally, the reversal learning paradigm. Each phase lasted about 8–30 trials, depending on the learning rate. Criterion for acquisition of each sub-task was set at 8 out of 10 correct digs and mice were excluded after not digging for 10 consecutive trials. The total duration of the experiment was 4 days. Four days prior to the start of the experiment, mice were food restricted up to

85% of their ad libitum body weight to ensure motivation to find the food reward for each of the phases.

Three chambers paradigm. The 3 chambers task was performed as previously described (Yang M, JL Silverman, et al. 2011). Briefly, mice were habituated to the central chamber of the box, which is divided in 3 similar, connected chambers. In the socialization phase, the mouse was allowed to interact with either an empty wired cage or a wired cage with an unfamiliar, genotype matched, mouse. In the familiarization phase, the mouse was able to interact with the previous mouse or a new, unfamiliar, genotype matched, mouse. Time spent sniffing in each room was measured by blind manual scoring with Observer software (ObserverXT 10.5).

Statistical analyses

Statistical analysis was carried out with IBM SPSS Statistics. P values below 0.05 were considered statistically significant. Data are presented as mean and SEM throughout the manuscript (Source data 1). Individual trial differences in behavior were determined using one-way ANOVA to test genotype effects. For repeated measurements, a repeated measures ANOVA was performed with 'time' as within-subjects factor and 'genotype' as between-subjects factor. In case of a significant *p* value, post-hoc comparisons were performed using one-way ANOVA to determine individual time point effects. The involuntary movements and SHIRPA scores were not normally distributed and therefore compared using the general linear model. Values three time the standard deviation above or below the mean were treated as statistical outliers and excluded from further analysis. Normality and variance tests were first applied to all experimental data. When data followed a normal distribution, paired comparisons were analyzed with *t*-test, while

multiple comparisons were analyzed using either ANOVA with post-hoc Bonferroni correction (equal variances) or the Welch test with *post-hoc* Games-Howell (different variances). A χ^2-test was applied to analyze the distribution of cells in layers.

References

Kalueff AV, Stewart AM, Song C, Berridge KC, Graybiel AM, Fentress JC. 2016. Neurobiology of rodent self-grooming and its value for translational neuroscience. Nat Rev Neurosci 17:45-59.

Kas MJ, de Mooij-van Malsen AJ, Olivier B, Spruijt BM, van Ree JM. 2008. Differential genetic regulation of motor activity and anxiety-related behaviors in mice using an automated home cage task. Behav Neurosci 122:769-776.

Kumar SS, Huguenard JR. 2001. Properties of excitatory synaptic connections mediated by the corpus callosum in the developing rat neocortex. J Neurophysiol 86:2973-2985.

Molenhuis RT, de Visser L, Bruining H, Kas MJ. 2014. Enhancing the value of psychiatric mouse models; differential expression of developmental behavioral and cognitive profiles in four inbred strains of mice. Eur Neuropsychopharmacol 24:945-954.

Poliak S, Salomon D, Elhanany H, Sabanay H, Kiernan B, Pevny L, Stewart CL, Xu X, Chiu SY, Shrager P, et al. 2003. Juxtaparanodal clustering of Shaker-like K+ channels in myelinated axons depends on Caspr2 and TAG-1. J Cell Biol 162:1149-1160.

Ting JT, Daigle TL, Chen Q, Feng G. 2014. Acute brain slice methods for adult and aging animals: application of targeted patch clamp analysis and optogenetics. Methods Mol Biol 1183:221-242.

Yang M, Perry K, Weber MD, Katz AM, Crawley JN. 2011. Social peers rescue autism-relevant sociability deficits in adolescent mice. Autism Res 4:17-27.

Yang M, Silverman JL, Crawley JN. 2011. Automated three-chambered social approach task for mice. Curr Protoc Neurosci 8:26.